Astron. Astrophys. 342, 131–152 (1999)

ASTRONOMY AND ASTROPHYSICS

Evolution of massive stars under new mass-loss rates for RSG: is the mystery of the missing blue gap solved?

Bernardo Salasnich[1], **Alessandro Bressan**[2], **and Cesare Chiosi**[3,1]

[1] Department of Astronomy, University of Padova, Vicolo dell'Osservatorio 5, I-35122 Padova, Italy
[2] Astronomical Observatory, Vicolo dell'Osservatorio 5, I-35122 Padova, Italy
[3] European Southern Observatory, Karl-Schwarzschild-Strasse 2, D-85748 Garching bei München, Germany

Received 18 November 1997 / Accepted 3 September 1998

Abstract. In this paper we present new models of massive stars based on recent advancements in the theory of diffusive mixing and a new empirical formulation of the mass-loss rates of red supergiant stars. The study is articulated in two main parts. First, by means of a simple diffusive algorithm, we amalgamate the results of complex studies on non local convection (overshooting region) by Xiong (1989) and Grossman (1996), and apply them to model the structure and evolution of massive stars in occurrence of mass loss by stellar winds according to the popular relationship by de Jager et al. (1988). Stars with initial mass in the range 6 to 120 $M_\odot$ and initial chemical composition [Z=0.008, Y=0.25] and [Z=0.020, Y=0.28] are followed from the zero age main sequence till core He-exhaustion. Particular attention is paid to the 20 $M_\odot$ star as the prototype of the evolution of massive stars in the luminosity (mass) interval in which both blue and red supergiants occur in the HR diagram (HRD). The models confirm that, in the evolution of a massive star with mass loss, the dimension of the H-exhausted core and the efficiency of intermediate mixing strongly affect the evolution during the subsequent core He-burning phase, the extension of the blue loops in particular. However, despite the new mixing prescription, also these models share the same problems of older models in literature as far as the interpretation of the observational distribution of stars across the HRD is concerned. In the second part, we examine possible causes of the failure and find that the rate of mass loss for the red supergiant stages implied by the de Jager et al. (1988) relationship under-estimates the observational values by a large factor. Revising the whole problem, we adopt the recent formulation by Feast (1991) based on infrared data, and take also into account the possibility that the dust to gas ratio varies with the stellar luminosity. Stellar models are then calculated with the new prescription for the mass-loss rates during the red supergiant stages in addition to the new diffusive algorithm. The models now possess very extended loops in the HRD and are able to match the distribution of stars across the HRD from the earliest to the latest spectral types both in the Milky Way, LMC and SMC. During the loop phase the surface abundance of helium is significantly enhanced with respect to the original value as suggested by observational data for blue supergiant stars. Finally, because the surface H-abundance can be lowered to the limit adopted to start the Wolf-Rayet phase (WNL type), we suggest that a new channel is possible for the formation of low luminosity WNL stars, i.e. by progenitors whose mass can be as low as 20 $M_\odot$, that have evolved horizontally across the HRD following the blue-red-blue scheme and suffering large mass loss during the red supergiant stages.

Key words: stars: mass-loss – stars: evolution

1. Introduction

Among the physical phenomena at the base of stellar models, convective mixing is perhaps the most difficult one to handle properly, even if it is likely to play the dominant role. Suffice it to recall the long debate about the choice of the stability criterion and the related phenomena of semiconvection and overshoot (Schwarzschild & Harm 1965). Convection theory grows more and more complicated, (Xiong 1979, 1984; Canuto & Mazzitelli 1991; Canuto 1992; Grossman & Narayan 1993; Canuto 1996; Grossman & Taam 1996), but its application to the stellar models still requires a great deal of over-simplification (Zahn 1991; Alongi et al. 1993; Deng 1993; Deng et al. 1996a,b; Ventura et al. 1998).

The impressive body of literature on the mixing schemes and their bearing on the structure and evolution of massive stars shows that mixing in stellar interiors is a complex phenomenon because different physical instabilities and mixing processes arise in different regions of a star (see Chiosi et al. 1992, Chiosi 1997 for exhaustive reviews of the subject). It is worth recalling here that, following core H-exhaustion, the possible occurrence of an intermediate convective layer and consequent modification of the chemical profile over there are strictly related to the adopted stability criterion, either Schwarzschild ($\nabla_r < \nabla_a$) or Ledoux ($\nabla_r < \nabla_a + \nabla_\mu$), with profound consequences for the subsequent core He-burning phase.

Another phenomenon playing an important role in the evolution of massive stars is mass loss by stellar wind. In early type stars, the radiation driven wind theory developed starting from the seminal studies of Lucy & Solomon (1970) and Castor et

Send offprint requests to: B. Salasnich

al. (1975), followed by Abbott (1982), Pauldrach et al. (1986), Owocki et al. (1988) and many others, until the magistral review article by Kudritzski (1997, and references) provides quantitative predictions for the mass-loss rates that find confirmation in the observational data. There are still several aspects to be clarified, for instance the very high ratio $\dot{M}v_\infty/Lc^{-1}$ observed in some Wolf-Rayet stars (see Hillier 1996 and references). The situation is much less settled with the late type supergiant stars, see the review by Lafon & Berruyer (1991), and much work on this subject refers to bright AGB stars. The most likely mechanism is radiation pressure on dust grains (see Kwok 1975; Gail & Sedlmayr 1987). The situation is further complicated by possible effects due to pulsation (see Willson 1988), and perhaps sound waves generated either by convection in the mantle of the stars or by pulsation at high eigenmodes (see Pijpers & Hearn 1989; Pijpers & Habing 1989).

In star more massive than say 30 $M_\odot$, the evolution is almost fully determined by mass loss starting from the H-burning phase (see. Chiosi & Maeder 1986). In the mass range 15-30 $M_\odot$, both internal mixing and mass loss affect the evolutionary path in the HRD, so that stars in this mass range are a workbench for testing theories of massive star structure and evolution, thanks also to the lucky circumstance that in the luminosity interval pertinent to a typical 20 $M_\odot$ star counts in the Solar Vicinity and in the Magellanic Clouds are fairly complete (see Massey 1997). Below 15 $M_\odot$, mass loss by stellar winds gets less important and the the evolution is mainly driven by mixing.

The comparison of extant theoretical models with observations indicates, however, severe points of disagreement, probably due to our poor knowledge of the above physical phenomena. The reader is referred to Chiosi (1997) for an exhaustive discussion of these topics and referencing. In brief, the distribution of stars across the HRD in the luminosity range $-7 \geq M_{\rm bol} \geq -9$ and the surface chemical abundances of these stars hint that after central H-exhaustion, a star should ignite core He-burning as a red supergiant (RSG), perform an extended blue loop up to the main sequence band, and eventually return to the RSG region, thus following the classical case A evolutionary scheme of Chiosi & Summa (1970). If we take the progenitor of SN1987a as an indicator of the final fate of the evolution of massive single stars, then the model should perform a final loop toward hotter temperatures during the central C-burning phase. No stellar model is found in literature able to fit this simple evolutionary scheme. In particular, the extension of the loop into the blue region is far too short with respect to what required by observations, and gives rise to the so called "Blue Hertzsprung Gap (BHG) problem". In fact, the theory predicts the existence of a gap between the core H- and He-burning regions caused by the long lifetime of the major nuclear phases and the short timescale passing from the first to the second one. Therefore, very few stars should fall in the gap. In reality the opposite occurs and the vast majority of blue supergiants crowd the *forbidden* area. Several ways out have been proposed in the past none of which is really able to unravel the mystery (see Chiosi 1997).

Furthermore, the predicted surface abundance of helium (and other elements as well) are too low as compared to the observational data (see Herrero et al. 1992, Venn 1995, Lennon et al. 1996).

Finally, there is the long debated problem of the origin of low luminosity WR stars. They are found in a region near the main sequence down to the luminosity of a typical 15 $M_\odot$ star. Low luminosity WR stars are currently understood as the descendants of the most massive stars ($\geq$ 30 $M_\odot$) that under the effects of a vigorous stellar wind lose their entire H-envelope and reach such low luminosities following the mass-luminosity relation (see Maeder & Conti 1994). However, first of all the predicted effective temperature of WR stars is by far higher than observed, and secondly the lifetime during which the evolutionary tracks populate the "observed" region is by far too short. Attempts to cure the disagreement were not particularly satisfactory.

In this study we thoroughly investigate the effects of mixing and mass loss on the structure and evolution of a typical 20 $M_\odot$ star in order to cast light on the coupling of the two phenomena in this mass range. The study is articulated in two main steps for the sake of better understanding. The first part deals with a new prescription for mixing and canonical rates of mass loss. Mixing is described by means of a diffusive algorithm easily applicable to stellar models. In the second part of the paper, we address to mass loss during the RSG stages showing that the prescriptions currently in use likely underestimate the observational mass-loss rates during this phase. A new prescription is proposed and incorporated in the stellar models with the new mixing formalism.

The plan of the paper is as follows. In Sect. 2 we present our formulation of diffusion and derivation of the diffusion coefficient, which takes different values throughout a star. In Sect. 3, first we describe the results obtained for our prototype model of 20 $M_\odot$ with particular emphasis on the value of the adopted parameters, and second we present two complete sets of stellar models with chemical composition [Z=0.020, Y=0.280] and [Z=0.008, Y=0.250]. The results are compared with observations, highlighting the points of uncertainty and disagreement that strongly hint for a new formulation of the mass-loss rate during the RSG phase. The new rates of mass loss are presented in Sect. 4 and are compared to the standard ones. In Sect. 5 we describe the results obtained with the revised mass-loss rates, and show how the new stellar models are able to improve sensitively upon the solution of the BHG problem. In Sect. 6, we tune the mixing parameters under the new mass-loss rates in the RSG phase and outline the role played by the mixing parameters and mass loss rates during the RSG in determining the path of a star in the HRD. In Sect. 7, by means of suitably designed experiments we investigate to which extent internal mixing and mass loss from RSG stage concur to determine the final result. It emerges that mass loss is the dominant factor. Finally, some concluding remarks are drawn in Sect. 8.

2. Mixing: the diffusive approach

Different kinds of convective instability may arise in different regions of a star in the course of its evolution, which require suitable descriptions of the ensuing mixing.

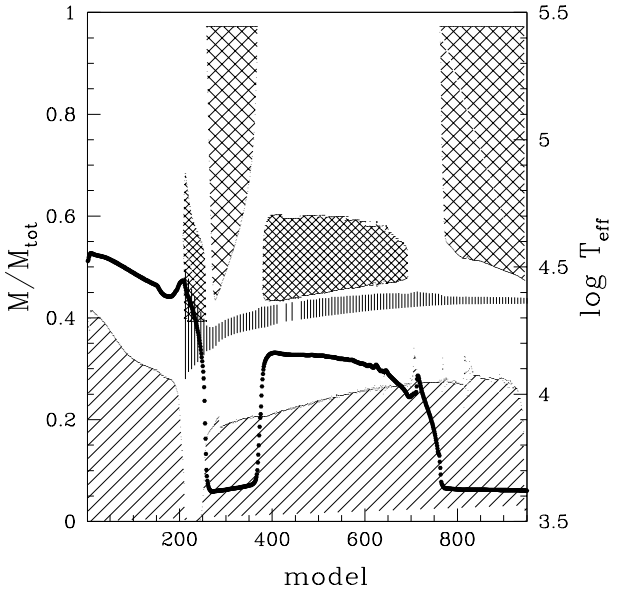

Fig. 1. Internal structure of the 20 $M_\odot$ star with chemical composition [Z=0.008, Y=0.250] as a function of the model. The single hatched regions correspond to the convective core defined by the Schwarzschild criterion, whereas the double hatched zones show the intermediate fully convective layers and the external convective envelope. The vertical lines display the extension of the H-burning shell. The boundaries are taken where the rate of nuclear energy release drops below 10^{-3} of the peak value. For the sake of clarity the overshoot regions around the core are not drawn, likewise for the overshoot region at the base of the external envelope and at the edges of the intermediate convective shell. Finally, the heavy dots show the run of the effective temperature in the course of evolution (right vertical axis).

The structure of a typical massive star of 20 $M_\odot$ from the main sequence to late core He-burning is displayed in Fig. 1. During the H-burning phase the star is composed by a convectively unstable core (the single hatched region) surrounded by formally stable radiative layers. Owing to the inertia of the convective elements, a significant fraction of the radiative region can be partially or totally mixed with the core, the so-called *overshooting*. As the evolution proceeds, above the H-burning core potentially unstable oscillatory convection may develop (Merryfield 1995), and eventually turn into *semiconvection* over extended regions, across which a suitable chemical profile is built up. In the same layers, at the beginning of shell H-burning, one or more fully convective zones may arise, depending on the adopted stability criterion (dense double-hatched areas in Fig. 1). These intermediate convective regions can even penetrate into the H-burning shell (vertical lines in Fig. 1). The whole structure is finally surrounded by an outer radiative (during the BSG stages) or convective (during the RSG stages) envelope (double hatched zones in Fig. 1).

In principle, each of these unstable regions is characterized by its own mixing time-scale (see Canuto 1994 and references therein). Therefore, the associated mixing is best described by a diffusive scheme (Weaver & Woosley 1978; Langer et al. (1983,1985); Deng 1993; Deng et al. 1996a; Gabriel 1995; Grossman & Taam 1996; Herwig et al. 1997; Ventura et al. 1998 and references therein).

The diffusion equation is

$$\frac{dX}{dt} = \left(\frac{\partial X}{\partial t}\right)_{nucl} + \frac{\partial}{\partial m_r}\left[(4\pi r^2\rho)^2 D \frac{\partial X}{\partial m_r}\right] \quad (1)$$

where the variation of the chemical abundance in a mesh point at time t due to nuclear burning has been singled out.

The corresponding time-scale of the mixing process over a distance L is

$$t_{diff} = L^2/D \quad (2)$$

The use of the diffusive algorithm in stellar model calculations offers two advantages: (i) Since mixing is a time-dependent process, the diffusive scheme takes into account the possibility of incomplete mixing over the time-step t_{evol} between two successive models. The region will be homogenized over a time interval much longer than the diffusive time-scale. (ii) Adopting a unique prescription, we can deal with different physical processes of mixing such as full convection, semiconvection, rotationally induced mixing, convective overshoot, that can occur in different regions of a star.

Following Deng et al. (1996a), we distinguish three main regions of a star, in which the treatment of mixing requires different prescriptions for the diffusion coefficient owing to the different physical nature of the process inducing mixing.

(a) *The homogeneous central region*

With this we mean the central core of the star which is unstable to convection according to the Schwarzschild criterion. As in this region the convective elements have the same probability of crossing the nuclear burning zone, no specific algorithm for mixing is required to make it homogeneous (see Deng 1993). In any case, the characteristic time of the homogenization process is of the order of the convective turnover time. In principle, this region should correspond to the very central sphere with radius equal to the mean free path of the elements. However, we will consider the whole central region unstable to convection as being homogenized over the convective time-scale, and hence adopt a diffusion coefficient able to secure complete mixing, i.e.

$$D = \frac{1}{3}(v \times L_c) \quad (3)$$

where v is the turbulent velocity calculated with the Mixing Length Theory (MLT) and L_c is the radius of the central unstable region. This is the expression adopted by Weaver & Woosley (1978), Langer et al. (1983, 1985), Deng (1993) and Deng et al. (1996a).

(b) *The overshoot region*

Hydro-dynamical modeling of stellar convection by Grossman (1996) shows that turbulent velocities may penetrate into the surrounding stable region with a decay scale which is of the order of one pressure scale height H_P [see also Grossman et al. (1993) for details].

Such a large extension of the overshoot region is consistent with the results by Xiong (1985), who showed that different physical quantities have different distance of penetration into the radiative region, and that their fluctuations decrease exponentially from the Schwarzschild border. In this regard, see Figs. 5a,b in Xiong (1985), Fig. 3 in Xiong (1989), and the 60 $M_\odot$ star in Xiong (1985), in which an e-folding distance of $1.4c_1H_P$ is found, where c_1 is the efficiency parameter of the energy transport. Assuming $c_1 = 0.5$ like in Xiong (1985), we obtain an e-folding distance of $0.7H_P$, which is comparable with the value suggested by Grossman (1996). Recent hydrodynamical simulations by Freytag et al. (1996) reveal that the transition from convective and hence mixed regions to those not affected by mixing is rather sharp due to the fast decline of the convective velocities, and confirm moreover that the velocity field continues beyond the region with significant convective flux, declining exponentially with the depth. Simulations of convective velocity field at the surface of a star (Freytag et al. 1996) suggest that the diffusion coefficient varies with the distance r from the border of the convective region according to

$$D = H_P v_0 \times exp[-2r/(H_v)] \tag{4}$$

where H_v and v_0 are the velocity scale height and velocity, respectively, at border of the convective zone. Furthermore, H_v is found to vary from $(0.25 \pm 0.05)\ H_P$ in models of A-type stars to $1.0 \pm 0.1 H_P$ in models of white dwarfs, thus indicating a significant dependence of the diffusion coefficient upon the type of star.

The above mentioned studies suggest that beyond the convective region turbulent velocities neither vanish abruptly (no overshoot) nor generate a fully mixed region (the standard picture of convective overshoot), but decay exponentially into the stable layers.

On the basis of these considerations, we assume that in the overshoot regions the diffusion coefficient declines exponentially with the distance from the border of the core, and adopt the pressure scale height as the critical distance over which mixing is effective:

$$D = \frac{1}{3} H_P v_0 \times exp[-r/(\alpha_1 H_P)] \tag{5}$$

with obvious meaning of the symbols. We introduce the parameter α_1 because in the original formulation by Xiong (1989) and Grossman (1996) (corresponding to $\alpha_1 \simeq 0.5$) the diffusion coefficient decreases too slowly yielding complete homogenization over too wide a region around the unstable core, and the resulting stellar models are unable to match most of the observational data (see the entries of Table 1 below).

(c) *The intermediate convective region*

Following central H-exhaustion an extended region with a gradient in molecular weight develops in which a convective zone may arise owing to the so-called *oscillatory convection or overstability*. The physics of this phenomenon has been studied by many authors by means of linear-stability analyses. In particular, Kato (1966) showed that, due to heat dissipation processes, in a region which is stable against convection according to the Ledoux criterion but not to the Schwarzschild criterion, infinitesimal perturbations grow on a time-scale of the order of the thermal diffusion time-scale t_{heat}, giving rise to oscillatory convection which eventually mixes the whole region.

It is thus conceivable that the diffusion coefficient in this region is governed by the thermal diffusion time-scale t_{heat}, which according to Langer et al. (1983, 1985) can be expressed as

$$t_{heat} = \frac{\varrho c_p}{K k^2} \tag{6}$$

where

$$K = \frac{4acT^3}{\chi \varrho} \tag{7}$$

is the radiative-conductivity coefficient, and k^{-1} is the characteristic scale-length of the perturbations, approximated here to H_P. All other symbols have their usual meaning.

Since we do not know when the perturbation becomes finite and what the real time-scale of the mixing process is, we express the diffusion coefficient as

$$D = L^2/t_{growth} \tag{8}$$

where L is the size of the intermediate convective zones as defined by the Schwarzschild criterion, and $t_{growth} = \alpha_2 \times t_{heat}$, where α_2 is a suitable constant to be determined by comparing theoretical results with observations.

With these assumptions it turns out that the diffusion coefficient D is weakly dependent on the size L of the intermediate convective zone, contrary to Langer et al. (1983, 1985) and Grossman & Taam (1996).

Complete mixing is ensured if $t_{growth} << t_{evol}$ (the characteristic evolutionary time-scale). In our modeling, the whole process is controlled by the parameter α_2. Fig. 2 shows the hydrogen content in four successive models during the Kelvin-Helmholtz phase, in which two extreme values for α_2 have been adopted, i.e. $\alpha_2 = 1000$ (right panels) and $\alpha_2 = 0.5$ (left panels). To better understand the effect of diffusion in this phase on the chemical profile generated in previous stages, we introduced a scalar quantity at the center of the unstable region and follow its evolution in the four models. This is shown in the upper panels of Fig. 2. These experiments are meant to illustrate the profile generated by diffusive mixing alone.

It is worth noticing that by varying α_2, the chemical profiles corresponding to the Schwarzschild (rectangular profile) and the Ledoux neutrality condition (smoothed profile) are recovered.

Finally for the sake of simplicity, we neglect overshooting from the intermediate convective shell into the adjacent radiative regions.

Summary of the prescriptions for D

We have presented a simple diffusive scheme suited to dealing with mixing in different convective regimes.

In the central unstable region the adopted diffusion coefficient (Eq. 3) secures complete homogenization on the nuclear

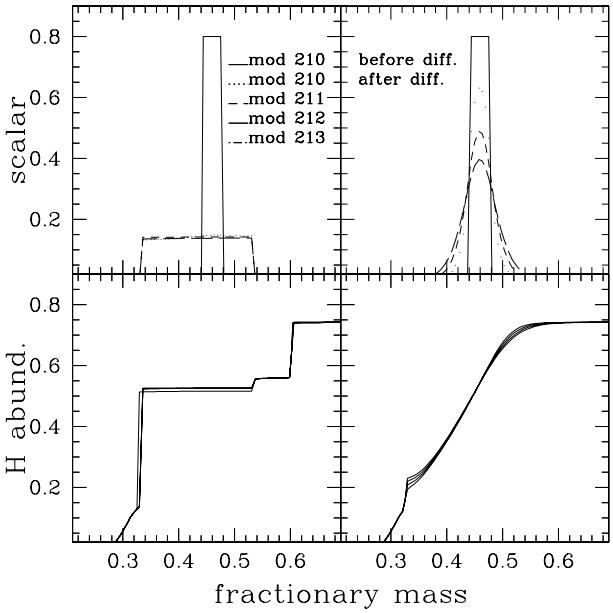

Fig. 2. Hydrogen abundance by mass (*bottom panels*) as a function of the fractionary mass of 4 successive models during the Kelvin-Helmholtz phase. The upper panels shows the diffusion of a scalar quantity arbitrarily introduced at the center of the intermediate convective region of the first model. The models are calculated with $\alpha_1 = 0.009$ and $\alpha_2 = 1000$ (*right panels*) and $\alpha_1 = 0.009$ and $\alpha_2 = 0.5$ (*left panels*) respectively.

time-scale. In the overshoot region the diffusion coefficient decays exponentially from the border of the Schwarzschild core, with a typical scale-length equal to $\alpha_1 \times H_P$. This choice is based on the results of recent hydro-dynamical studies showing that convective turbulent velocities decay exponentially into the surrounding stable radiative region. Notice that instead of specifying a characteristic length of the overshoot region we specify the scale-length of the decay of the overshoot process, which sounds to be more physically grounded. Since current theoretical predictions seem to over-estimate the decay length, we introduce a parameter α_1 to be eventually calibrated on the observations.

In the intermediate convective region which may develop in layers with a gradient in chemical abundances (built up in previous stages according to the Schwarzschild criterion), we adopt a diffusion coefficient based on a fraction of the thermal dissipation time-scale ($t_{growth} = \alpha_2 \times t_{heat}$). By changing the parameter α_2 we may recover the Schwarzschild or the Ledoux criterion for convective stability. This diffusive scheme secures that complete mixing occurs only when $t_{growth} << t_{evol}$.

3. Stellar models with the new mixing scheme

In this section we present stellar models calculated with the above prescriptions for internal mixing. Prior to this, we perform a detailed study of a typical 20 $M_\odot$ star in order to check the response of the stellar structure to variations of the parameters α_1 and α_2. We adopt the chemical composition [Z=0.008, Y=0.25], which is most suited to stars in the LMC (see below). The evolution is followed from the main sequence till the core He- exhaustion stage.

In order to proceed further, we first need to specify the prescription adopted for the mass-loss rate throughout the various evolutionary phases. All other details concerning the input physics (opacity, nuclear reaction rates, neutrino energy losses, etc.) are as in Fagotto (1994), to whom the reader is referred.

3.1. Mass-loss rates: the canonical prescription

Throughout the various evolutionary phases up to the so-called de Jager limit the mass-loss rates are from the popular compilation by de Jager et al. (1988), although we are aware that Lamers & Cassinelli (1996) have recently emphasized that the de Jager et al. (1988) sample is heavily affected by selection effects, proposing a new expression of $\dot{M}$ for early type stars. Our choice is motivated by the request of homogeneity with previous work to which the present models are compared.

Beyond the de Jager limit, the mass-loss rate is increased to $10^{-3}\mathrm{M}_\odot\mathrm{yr}^{-1}$, as suggested by observational data for the LBV (Maeder & Conti 1994).

As far as the dependence of the mass-loss rates on metallicity is concerned, we scale the rates according to $(Z/Z_\odot)^{0.5}$, as indicated by the theoretical models of stellar wind by Kudritzky et al. (1989). We adopt this formulation for the sake of comparison with Fagotto et al. (1994) though the observational data suggest a slightly steeper trend, see Fig. 1 in Lamers & Cassinelli (1996). Note also that theoretical mass-loss rates for the most massive stars could be down by a significant factor with respect to the real ones (de Koter et al. 1997).

The WNL stage of WR stars is assumed to start when the surface abundance of hydrogen falls below X=0.40, as in Maeder (1990). In this phase we adopt $\dot{M} = 10^{-4.4}\mathrm{M}_\odot\mathrm{yr}^{-1}$. During the subsequent WNE and WC phases, determined by the condition on the abundances $\mathrm{X} < 0.01$ and $\mathrm{C_{sup}} > \mathrm{N_{sup}}$ (by number) respectively, we apply the type-independent relation

$$\dot{M} = 0.8\ 10^{-7}(M/M_\odot)^{2.5}, \tag{9}$$

a mean between the values proposed by Langer (1989) for each sub-group.

The above prescriptions for the mass-loss rate are of general application and not meant for the 20 $M_\odot$ star alone. We anticipate however, that the 20 $M_\odot$ star always remains in the de Jager et al. (1988) regime, and that its mass-loss rates during the RSG phase are significantly lower than observed. In particular, the rates are lower by a factor of 5 as compared to the estimate by Feast (1991) for a sample of RSG stars (see below).

3.2. Results for the 20 $M_\odot$ star

As already anticipated, there is a growing amount of evidence suggesting that a typical 20 $M_\odot$ star with the chemical composition of the LMC should evolve according to the evolutionary scheme of case A after Chiosi & Summa (1970), which is characterized by an extended loop across the HRD during the central He-burning phase. This is substantiated by observed sur-

Table 1. Stellar models with the new prescription for the diffusive mixing, standard mass-loss rates, and chemical composition [Z=0.008, Y=0.25]. See the text for more details.

		A		B		LOOP								
α_1	α_2	$logL$	$logT_{eff}$	$logL$	$logT_{eff}$	$logL$	$logT_{eff}$	Q_{HE}	Q_{XP}	Q_{XD}	$t_H \cdot 10^6$	$t_{He} \cdot 10^6$	t_{He}/t_H	CASE
0.0001	1	4.58	4.51	4.98	4.41	–	–	0.094	0.300	0.524	8.179	1.139	0.139	B
0.009	0.001	4.58	4.51	4.98	4.41	–	–	0.163	0.407	0.518	8.975	0.920	0.102	B
	1	4.58	4.51	4.98	4.41	–	–	0.163	0.407	0.518	8.975	1.171	0.130	B
	4	4.58	4.51	4.98	4.41	–	–	0.163	0.407	0.518	8.975	1.279	0.142	B
	5	4.58	4.51	4.98	4.41	–	–	0.163	0.407	0.518	8.975	1.155	0.128	B
	100	4.58	4.51	4.98	4.41	–	–	0.163	0.407	0.518	8.975	0.851	0.095	B
	500	4.58	4.51	4.98	4.41	5.12	3.89	0.163	0.407	0.518	8.975	0.915	0.112	A
	800	4.58	4.51	4.98	4.41	–	–	0.163	0.407	0.518	8.975	1.050	0.117	C
0.015	5	4.58	4.52	5.02	4.39	–	–	0.206	0.447	0.541	9.520	0.854	0.089	C
	40	4.58	4.52	5.02	4.39	–	–	0.206	0.447	0.541	9.520	0.867	0.091	C
	45	4.58	4.52	5.02	4.39	5.17	4.25	0.206	0.447	0.541	9.520	0.847	0.089	A
	100	4.58	4.52	5.02	4.39	5.17	4.26	0.206	0.447	0.541	9.520	0.995	0.104	A
	120	4.58	4.52	5.02	4.39	–	–	0.206	0.447	0.541	9.520	0.835	0.087	C
	200	4.58	4.52	5.02	4.39	–	–	0.206	0.447	0.541	9.520	0.817	0.085	C
0.018	20	4.58	4.52	5.04	4.38	–	–	0.238	0.464	0.562	9.805	0.783	0.079	C
	50	4.58	4.52	5.04	4.38	5.18	4.12	0.238	0.464	0.562	9.805	0.805	0.082	A
	100	4.58	4.52	5.04	4.38	5.18	4.16	0.238	0.464	0.562	9.805	0.837	0.085	A
	280	4.58	4.52	5.04	4.38	5.18	4.06	0.238	0.464	0.562	9.805	0.815	0.083	A
	300	4.58	4.52	5.04	4.38	–	–	0.238	0.464	0.562	9.805	0.845	0.086	C
	400	4.58	4.52	5.04	4.38	–	–	0.238	0.464	0.562	9.805	0.762	0.077	C
0.021	0.1	4.58	4.51	5.06	4.36	–	–	0.264	0.486	0.587	10.060	0.872	0.086	C
	1	4.58	4.51	5.06	4.36	5.20	4.11	0.264	0.486	0.587	10.060	0.839	0.083	A
	5	4.58	4.51	5.06	4.36	5.20	4.19	0.264	0.486	0.587	10.060	0.983	0.097	A
	50	4.58	4.51	5.06	4.36	5.20	4.21	0.264	0.486	0.587	10.060	0.759	0.075	A
	300	4.58	4.51	5.06	4.36	5.19	4.05	0.264	0.486	0.587	10.060	0.746	0.074	A
	500	4.58	4.51	5.06	4.36	–	–	0.264	0.486	0.587	10.060	0.746	0.074	C
0.027	50	4.58	4.51	5.11	4.33	–	–	0.310	0.528	0.633	10.573	0.745	0.070	C
0.05	100	4.58	4.51	5.21	4.30	–	–	0.415	0.659	0.755	13.571	–	–	-

face abundances of blue supergiant stars, suggesting that they have already undergone the first dredge-up episode in the RSG phase.

Given these premises, many evolutionary sequences of the 20 $M_\odot$ star have been calculated for different choices of the parameters α_1 and α_2 to understand under which circumstances the above evolutionary scheme is recovered. The results are reported in Table 1. Columns (1) and (2) of Table 1 list the parameters α_1 and α_2 adopted for each sequence. Columns (3) through (8) are grouped according to the evolutionary stage; they refer to: the zero age main sequence (ZAMS), the stage of minimum effective temperature during central H-burning (TAMS), the largest extension of the loops, if present (LOOP). For each stage luminosity and effective temperature are listed. Columns (9), (10), and (11) list the following quantities: Q_{HE}, the fractionary mass of the He-core at central H exhaustion; Q_{XP}, the fractionary mass at the mid point throughout the region with a chemical gradient as seen at the core H-exhaustion stage; Q_{XD}, the fractionary mass of the layer at which the H-abundance starts to vary from surface values as seen at the H-exhaustion stage. Columns (12) and (13) list t_H and t_{He}, i.e. the duration of the H-burning and He-burning phases, respectively (lifetimes in units of 10^6 yr). Column (14) is the He- to H-burning lifetime ratio. Finally Column (15) lists the type of each evolutionary sequence according to the below classification scheme.

From the entries of Table 1, three evolutionary regimes are envisaged:

Case A: after the main sequence phase the star evolves to the RSG phase, performs an extended blue loop and completes He-burning as a RSG again. This corresponds to the models of Chiosi & Summa (1970) in which no mass loss and the Ledoux neutrality criterion for semiconvection were adopted.

Case B: after the main sequence phase the star begins the central He-burning phase as a BSG and slowly moves toward the red side of the HRD, where it ends the He-burning as a RSG. This corresponds to the models of Chiosi & Summa (1970) in which no mass loss and the Schwarzschild neutrality condition for semiconvection were adopted.

Case C: in this case the star spends the whole He-burning phase as RSG, corresponding to models with large and full overshoot. See also Bressan et al. (1993) with $\Lambda_c = 1$ in their formulation.

The other important feature of the stellar tracks to look at is the extension of the BHG predicted by the theory. From the 20 $M_\odot$ star models contained in Table 1, we can draw the following conclusions:

(1) A large value of α_1 yields a large extension of the overshoot region and hence a big H-exhausted core (Q_{HE}). As long known this causes a large extension of the main sequence band, a high luminosity during it and subsequent phases and, finally, a long H-burning lifetime. The models presented in Table 1 show complete mixing in the overshoot region up to a distance $\approx 13\alpha_1 H_P$ from the Schwarzschild border (estimated from $t_{diff} = t_{evol}$). Therefore they range from the no overshoot case ($\alpha_1 = 0.0001$) to the extreme overshoot case ($\alpha_1 = 0.05$), the latter case corresponding to the models of Bressan et al. (1981).

(2) The size of the core at the H-exhaustion stage is the factor dominating the entire subsequent evolution in the HRD. In fact, independently of α_2, i.e. the mixing efficiency in the intermediate convective zones, the models with $\alpha_1 \geq 0.015$ begin the He-burning phase as red supergiants, while the models with $\alpha_1 \leq 0.0001$ (no overshoot) do it as blue supergiants.

(3) The models with $\alpha_1 = 0.009$ are of particular interest because they represent a transition case. All the three schemes B, A, C are indeed recovered by increasing the value of α_2, i.e. by decreasing the efficiency of mixing inside the intermediate convective zone. We note that the fractionary core mass at central H-burning exhaustion is $Q_{HE} = 0.163$, very close to the value 0.161 obtained by Deng (1993) with $P_{diff} = 0.4$ in his formulation.

(4) Although the loop phenomenon eludes simple physical interpretations as pointed out long ago by Lauterborn et al. (1971), the models we have calculated indicate that when $0.009 \leq \alpha_1 \leq 0.021$ extended loops are possible.

Many of the results we have obtained apparently agree with those by Langer et al. (1989), however with major points of difference. The models by Langer et al. (1989) show indeed a similar trend in the HRD at varying his parameter α (models of type B and C are obtained for $\alpha > 0.01$ and and $\alpha < 0.008$ respectively). However, the prescription by Langer et al. (1989) and Langer (1991) does not favor the occurrence of convective overshooting. In fact, in presence of even modest overshoot (0.15 H_P corresponding roughly to $\alpha_1 = 0.009 - 0.015$ in our formalism), the models are always of type C so that they hardly match the observations.

Table 2 adds to the data of Table 1 the information about the surface abundances of the stellar models. We list the ratios of the surface abundances of ^{4}He, ^{12}C, ^{16}O, ^{14}N with respect to their initial values. The abundances are given at the stage of central He-exhaustion, Columns (3) through (6), and while the models are in the blue loop, Columns (7) through (10).

By inspecting Tables 1 and 2 we suggest that α_1=0.015 and α_2 in the range 50 to 100 should yield stellar models best matching the general properties of the HRD of massive stars in the luminosity range $-7 \geq M_{Bol} \geq -9$. In fact, the blue loops acquire then their maximum extension and the surface abundances of He and CNO elements are in good agreement with observations, e.g. Fitzpatrik & Bohannan (1993). For slightly lower values of α_1 the blue loops shrink and, more important, the surface abundance of He and CNO elements are only in very marginal agreement with observations. The situation gets worst at increasing α_1. Finally, values of $\alpha_1 > 0.021$ can certainly be excluded as they always lead to C-type models.

The case α_1=0.015 corresponds to a completely mixed overshoot region of about 0.2 H_P above the Schwarzschild border. *This value is significantly smaller than what is suggested by the hydro-dynamical models of Grossman and Xiong. Had we adopted $\alpha_1 \simeq$0.5 as indicated by the former studies, we would have gotten only the case C evolution, in disagreement with the observed distribution of stars across the HRD.* This result implies that some important ingredients are still missing in the original formulation of the mixing scale-length by Grossman (1996). It is worth noticing that Bressan et al. (1993), Fagotto et al. (1994) and the Geneva group (Charbonnel et al. 1993, Schaerer et al. 1993) adopt 0.25 H_P above the Schwarzschild border, a value that corresponds to about α_1=0.018. This explains why the extension of the blue loops of those models was always too short or missing at all.

Values of α_2 for which extended blue loops do occur are generally much larger than 1. *This indicates that the characteristic time of the mixing process is larger than the thermal dissipation time-scale or equivalently the growing time of the oscillatory convection.* Full mixing inside the intermediate unstable region, i.e. the straight application of the Schwarzschild criterion, is excluded by the present computations. However, no mixing at all can be also excluded, because the corresponding models would behave as in case C. Therefore, we are inclined to conclude that the characteristic time of the mixing process in this region is slightly longer than the Kelvin-Helmholtz lifetime. In other words, after central H-exhaustion, by the time perturbations grow in the intermediate unstable region the star has already evolved into the RSG phase.

Finally, our calculations show that the occurrence of the BHG is a general feature of all these evolutionary sequences. In fact, a BHG about Δ Log T_{eff}=0.1 wide is always predicted to exist between the maximum extension of the main sequence band and the hottest point of the He-burning phase. Because the models in Table 1 span quite a large range of mixing efficiencies both in the overshoot and intermediate convective region, we are convinced that an important physical ingredient is either still missing or badly evaluated in the stellar models of massive stars. We will come back to this problem later.

Table 2. Surface abundances by mass for the models of 20 $M_\odot$ and chemical composition [Z=0.008, Y=0.25]. The initial values of the abundances are: He=0.25 C=0.1371e-2 O=0.3851e-2 N=0.4238e-3.

α_1	α_2	He/He_i	C/C_i	O/O_i	N/N_i	He/He_i	C/C_i	O/O_i	N/N_i
0.0001	1	1.301	0.5446	0.8052	4.151	–	–	–	–
0.009	0.001	1.211	0.6629	0.8611	3.275	–	–	–	–
	1	1.3	0.581	0.8068	4.016	–	–	–	–
	4	1.334	0.5588	0.7868	4.259	–	–	–	–
	5	1.309	0.5504	0.792	4.257	–	–	–	–
	100	1.168	0.672	0.878	3.117	–	–	–	–
	500	1.179	0.6377	0.8689	3.325	1.024	0.8344	0.9771	1.728
	800	1.207	0.608	0.8486	3.598	–	–	–	–
0.015	5	1.231	0.6446	0.8333	3.568	–	–	–	–
	40	1.27	0.6187	0.8063	3.893	–	–	–	–
	45	1.335	0.423	0.7123	5.352	1.290	0.6004	0.7928	4.070
	100	1.391	0.3535	0.6723	5.911	1.298	0.5931	0.7873	4.141
	120	1.245	0.6424	0.8239	3.662	–	–	–	–
	200	1.265	0.6215	0.8099	3.853	–	–	–	–
0.018	20	1.292	0.6164	0.7886	4.037	–	–	–	–
	50	1.356	0.3799	0.7003	5.609	1.327	0.5794	0.7627	4.387
	100	1.322	0.5233	0.7673	4.519	1.314	0.5964	0.7728	4.240
	280	1.296	0.6004	0.7832	4.129	1.295	0.6067	0.7834	4.113
	300	1.274	0.6232	0.7993	3.924	–	–	–	–
	400	1.275	0.6163	0.7951	3.981	–	–	–	–
0.021	0.1	1.395	0.5602	0.7278	4.747	–	–	–	–
	1	1.344	0.5712	0.7525	4.485	1.334	0.5921	0.7543	4.405
	5	1.344	0.4958	0.7541	4.693	1.334	0.5921	0.7543	4.405
	50	1.327	0.5196	0.7543	4.618	1.327	0.5918	0.7543	4.398
	300	1.248	0.6372	0.8016	3.839	1.248	0.6372	0.8019	3.839
	500	1.248	0.6372	0.8016	3.839	–	–	–	–

3.3. The whole sets of stellar models

Adopting the parameters α_1=0.015 and α_2=50 indicated by the previous analysis of the 20 $M_\odot$ star, we have computed two sets of evolutionary tracks with initial masses 6, 7, 8, 10, 12, 15, 20, 30, 40, 60, 100, 120 $M_\odot$ and chemical composition [Z=0.008, Y=0.25] and [Z=0.020, Y=0.28]. Extensive tabulations of the main physical quantities for all these stellar models are not given here for the sake of brevity. They are available from the authors upon request.

The evolutionary path (solid lines) of these stellar models on the HRD are shown in Figs. 3 and 4 for Z=0.008 and Z=0.02, respectively. They are compared with the corresponding models computed with mild overshoot (dotted lines) by Fagotto et al. (1994) and Bressan et al. (1993).

The main sequence band of the new models is slightly narrower than in the case of the older tracks. This follows from the adopted value of α_1 which corresponds to a smaller overshoot distance.

Although the fully mixed region in the models with diffusion is smaller than in the old ones with straight homogenization, the amount of fuel brought into the region of nuclear reactions combined with a slightly lower luminosity produce an almost equal H-burning lifetime. This is shown by Fig. 5 where the lifetimes t_H and t_{He} for diffusive, classical semiconvective, and straight overshoot models are plotted as a function of the initial mass of the stars (top panel for Z=0.02, bottom panel for Z=0.008). This fact suggests that part of the inner chemical profile is due to diffusion itself and not to the receding of the convective core as the evolution proceeds.

The smaller H-exhausted cores of the new models yield a lower luminosity and in turn a longer core He-burning lifetime. Note in Fig. 5 that, while the H-burning lifetime of the models with diffusion is almost equal to that of models with straight overshoot and longer than that of models with semiconvection alone, the trend is reversed for the He-burning phase.

Without performing a detailed comparison of the new models with the observational properties of the HRD in the LMC and Solar Vicinity, which is beyond the scope of the present study, yet a number of conclusions are possible by simply examining the evolutionary tracks.

(1) The BHG is narrow in the case of the LMC metallicity, but it is dramatically large in the case of solar metallicity. With the adopted parameters, the 20 $M_\odot$ star with Z=0.02 follows case C evolution, which is at odd with the stellar census across the HRD of the Solar Vicinity.

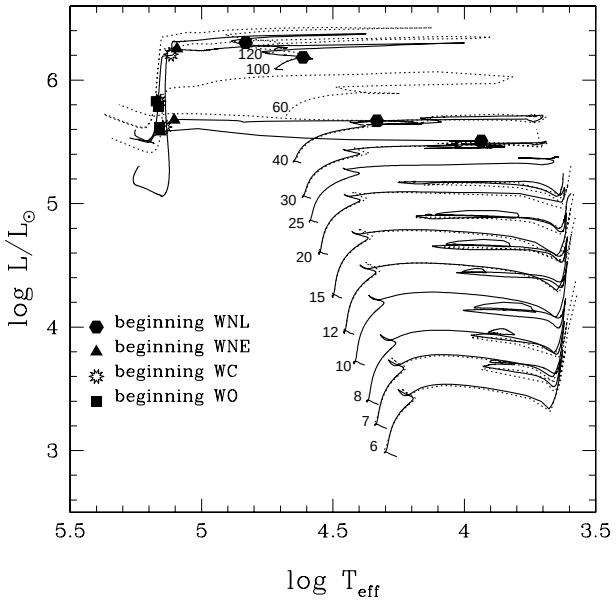

Fig. 3. The set of evolutionary tracks with composition [Z=0.008, Y=0.25] calculated with the new prescription for diffusive mixing for $\alpha_1 = 0.015$ and $\alpha_2 = 50$ (solid lines). They are compared with the tracks by Fagotto et al. (1994) with standard overshoot (dashed lines). The rate of mass loss during the various phase follow the standard scheme (see the text for more details).

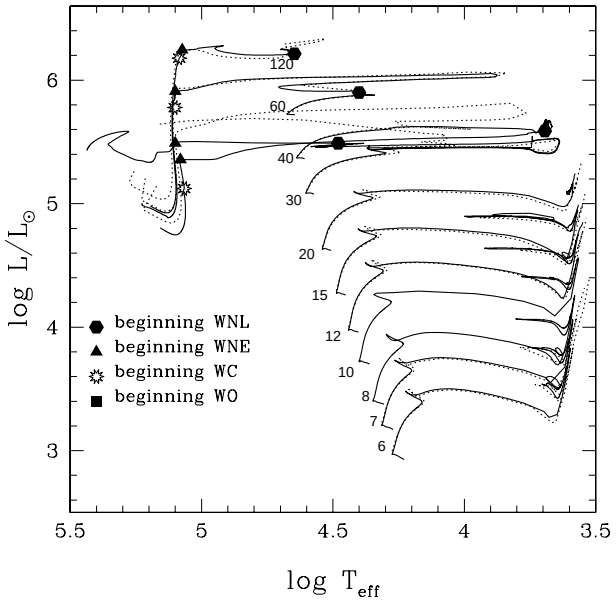

Fig. 4. The same as in Fig. 3 but for the chemical composition [Z=0.02, Y=0.28]. The new stellar models are compared with those by Bressan et al. (1993) with the same composition (dashed lines).

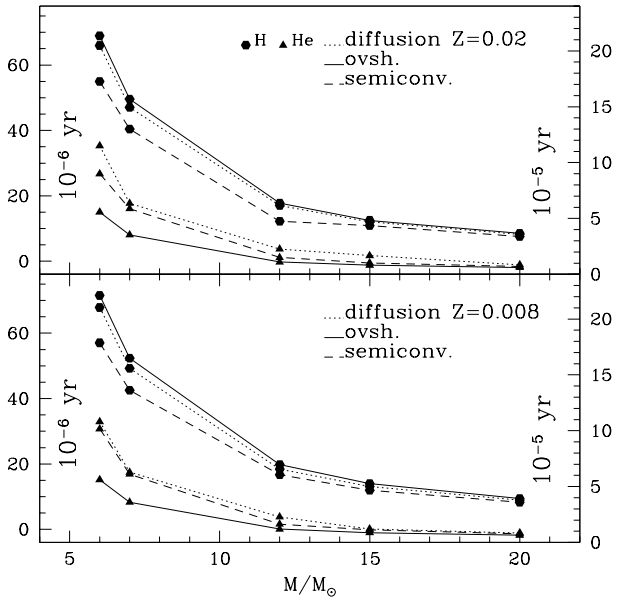

Fig. 5. Comparison of the lifetimes of the core H- and He-burning phases for the models with the new diffusive scheme (dotted lines) classical semiconvection (dashed lines) by Bressan et al. (1993), and standard overshooting (solid lines) by Fagotto et al. (1994). The diffusive models are for $\alpha_1 = 0.015$ and $\alpha_2 = 50$. The *top panel* is for the chemical composition [Z=0.020, Y=0.28], whereas the *bottom panel* is for [Z=0.008, Y=0.25]. The H-burning lifetimes (full dots) are in units of 10^6 yr (left vertical axis). The He-burning lifetimes (full triangles) are in units of 10^5 yr (right vertical axis)

(2) As long known, the evolution of the most massive stars (M $\geq 30 \div 40$ M$_\odot$) is dominated by mass loss rather than internal convection (see Chiosi & Maeder 1986; Chiosi et al. 1992). In this regard, the present models of 30-120 M$_\odot$ stars are much similar to the previous ones, in which similar prescriptions for the mass-loss rate were adopted. Perhaps the most intrigued problem in regard to the overall scenario of massive star evolution is the existence of WR stars and their genetic relationships with the remaining population of luminous (massive) stars. There is nowadays a general consensus that WR stars are the descendants of massive stars in late evolutionary stages. However, extant theoretical models of WR stars do not fully agree with their observational counterparts. In particular, it is hard to explain the location of low-luminosity WR stars. The problem is illustrated in Fig. 6, which compares the present evolutionary models for Z=0.02 with the data for galactic WN stars from Hamann et al. (1993). Surprisingly, WN stars populate a region which coincides with the main sequence band in the luminosity range $4.5 \leq \log L/L_\odot \leq 6$. WNL stars, indicated by triangles, populate the bright end of the distribution ($5.2 \leq \log L/L_\odot$), whereas WNE stars populate the faint end ($\log L/L_\odot \leq 5.5$). In contrast, extant theoretical models predict that WNL stars should evolve horizontally up to $\log T_{\rm eff} \simeq 5.1$. Note that, with the adopted mass-loss rates, no WNL-like model is fainter than $\log L/L_\odot \simeq 5.5$. The problem gets worse for WE stars, because they are predicted at $\log T_{\rm eff} \geq 5.1$ and often brighter than $\log L/L_\odot = 5.1$, hence much hotter (and brighter) than observed.

It has been argued that the discrepancy in the effective temperature can be cured by applying the well known correction taking into account departure from hydrostatic equilibrium and optical thickness in an expanding atmosphere. In fact, the photosphere of an expanding dense envelope can be different from that of a hydrostatic model (see Bertelli et al. 1984 and refer-

ences therein). However, only a fraction of the observed WNE stars shows evidence of a thick atmosphere (circles in Fig. 6), while the majority do not. Therefore, our hydrostatic models seem to be adequate to the present aims.

In addition, it has been suggested that current theoretical predictions of the mass-loss rate among the most massive O stars are down by a significant factor with respect to observed values (de Koter et al. 1997). In fact Meynet et al. (1994), adopting a mass-loss rate during the whole pre-WNE phase which is twice as much as the rate provided by the standard de Jager et al. (1988) prescription, obtain a better agreement as far as the observed WR/O ratio is concerned (Maeder & Meynet 1994), and get a fainter luminosity during the WC and WO phases. However they run into the same problem as far as low luminosity WN stars are concerned.

The same difficulty is encountered even by more sophisticated models, which combine the interior structure with a realistic expanding atmosphere. The reader is referred to Fig. 8 and related discussion in Schaerer (1996) for more details.

Finally, the ratio between the number of massive stars still on the main sequence and the number of WR stars observed in galaxies of the Local Group is ~ 3, and among other things independent of metallicity (Massey et al. 1995a,b; Massey 1997). In contrast, the nuclear time-scales involved suggest a ratio of $\sim$10, thus indicating that under a normal initial mass function the lowest mass for WR progenitors is smaller than about 40 $M_\odot$ (see Table 14 in Massey et al. 1995b) for the field stars in LMC. A cautionary remark is worth being made here as the number ratios above could change in the light of the recent reclassification of WR stars in R136a (de Koter et al. 1997).

The results of this section can be summarized as follows

- Even these new stellar models cannot reproduce the observed distribution of O-B-A stars in the HRD in the luminosity interval $-7 \leq \mathrm{M_{Bol}} \leq -9$ (the BHG problem) and the distribution of low luminosity WN stars.
- Although a complete exploration of the parameter space has not been performed, yet the models computed with different mixing efficiency in their convectively unstable zones hint that mixing alone cannot solve the problem.
- *Is mass loss the great villain of the whole story? And could higher rates of mass loss expose inner layers to the surface even in the mass range* $15 \div 30$ $M_\odot$*?*

Recalling past work along this vein, Bertelli et al. (1984) were able to produce evolutionary tracks of a 20 $M_\odot$ model with the suitable low surface hydrogen abundance, corresponding to a WN star, through the combined effect of an enhancement in the opacity around one million K^o and a constant mass-loss rate of a few 10^{-5} $M_\odot$/yr during the RSG phase.

More recently Bressan (1994) suggested that a larger mass-loss rate in the RSG phase and a suitable treatment of internal mixing could, at least for the model of 20 $M_\odot$ and solar abundance, lead a star to abandon the RSG region and display the features of a WN star. He noticed that strong support to this idea comes from the mass-loss rates for RSG stars reported by Feast (1991).

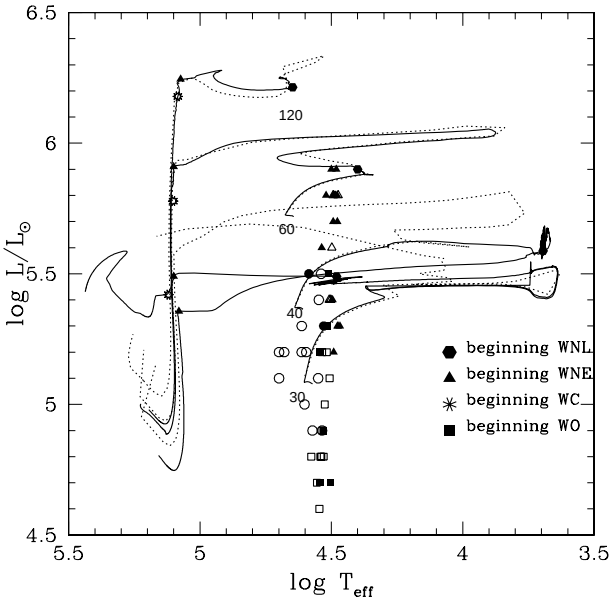

Fig. 6. Comparison of the evolutionary tracks with composition [Z=0.02, Y=0.28] and diffusion ($\alpha_1 = 0.015$, $\alpha_2 = 50$) during their WR stages and the observed WNL and WNE stars by Hamann et al. (1993). The data (triangles, circles and squares) refer to WNL, $\mathrm{WNE_s}$ and $\mathrm{WNE_w}$ stars, respectively. Full symbols are WR stars with detected hydrogen, whereas empty symbols stand for WR stars with no hydrogen.

4. New mass-loss rates in the RSG phase

The considerations made in the previous section suggest a reexamination of the mass-loss rates adopted during the red supergiant phase for stars in the mass range 10 to 30 $M_\odot$.

It is known (Chiosi & Maeder 1986; de Koter et al. 1997) that mass-loss rates in the upper end of the HRD are uncertain by a large factor. This is particularly true for red supergiant stars, where the mass-loss rate is estimated from a semi-empirical relation obtained by Jura (1986) for the AGB stars. Uncertainties in the above relation are due to the distance of the objects and the gas to dust ratio adopted to convert the dust mass-loss rate into the total mass-loss rate.

The average value of the mass-loss rate of RSG stars of the LMC is $3.6 \cdot 10^{-5}\mathrm{M_\odot/yr}$ (see Table 5 in Reid et al. 1990), whereas the value derived from the de Jager et al. (1988) formulation for a typical 20 $M_\odot$ model with $\log \mathrm{T_{eff}}$=3.6 and $\log \mathrm{L/L_\odot}$=5.0 is to $\dot{\mathrm{M}} \sim 10^{-6}\mathrm{M_\odot/yr}$.

Recently, Feast (1991) found a tight correlation between the mass-loss rate and the pulsational period in RSG stars of the LMC:

$$log(\dot{M}) = 1.32 \times logP - 8.17 \qquad (10)$$

where P is in days.

A similar empirical relation has been proposed by Vassiliadis & Wood (1993) for Mira and OH/IR stars, and has been applied to the evolution of AGB stars. This relation breaks down when the star reaches a pulsational period of about 500 days; afterward the mass-loss rate increases at a much slower rate or

even remains constant with the period. Remarkably in this second stage, the so called super-wind phase, the mass-loss rate reaches about the value one would obtain by equating the gas-momentum flux to radiation-momentum flux.

On the theoretical side, hydro-dynamical models by Bowen & Willson (1991) and Willson et al. (1995) show that shock waves generated by the large amplitude pulsations in AGB stars levitate matter out to a radius where dust grains can condensate; after this stage, radiation pressure on grains and subsequent energy re-distribution by collisions accelerate the matter beyond the escape velocity.

A thorough discussion of the problem, in particular whether the ratio between the two fluxes may be of the order of unity, can be found in Ivezic & Elitzur (1995).

Assuming the distance modulus to the LMC (m-M)=18.5, and combining Eq. (10) with the following empirical relation between the bolometric magnitude and the pulsational period (Feast 1991)

$$M_{bol} = -2.38 \times logP - 1.46 \tag{11}$$

we obtain the relation between the mass-loss rate and the luminosity of the star:

$$log(\dot{M}) = -11.59 + 1.385\ log(\frac{L}{L_{\odot}}) \tag{12}$$

Relation (12), hereinafter referred to as the *Feast Relation*, is shown in Fig. 7 (heavy dashed line) together with the mass-loss rate obtained with de Jager et al. (1988) for different effective temperatures (thin dashed lines).

In addition to this, we plot also the mass-loss rates for the super-wind phase (hatched areas):

$$\dot{M} = 6.070 \times 10^{-3}\ \beta\ \frac{L}{cv_{\rm exp}} \tag{13}$$

where the mass-loss rate is in $M_{\odot}$ yr^{-1}, the luminosity L is in solar units, the expansion velocity is $v_{\rm exp}$ = 15 Km s^{-1} and c is the light speed in Km s^{-1}. β is a quantity of order of unity, in which, following the empirical calibration by Bressan et al. (1998), we include the metallicity dependence

$$\beta = 1.13 \times \frac{Z}{0.008} \tag{14}$$

Note that in the luminosity range characteristic of RSG stars ($\log L/L_{\odot} \approx 4 \div 5.4$) the mass-loss rate computed according to Feast (1991), Eq. (12), is about a factor of ten larger than the predicted by the de Jager et al. (1988) formulation. This difference gives an idea of the uncertainty with which the rates are presently known. Tracing back the causes of this discrepancy is beyond the scope of the present paper. However we notice that, while the Feast (1991) formulation ultimately depends on the luminosity of the star, the relation by de Jager et al. (1988) contains also the effective temperature. If for any reason the models fail to reproduce the correct effective temperature of RSG stars (indeed the models are bluer than the real stars, a long known problem), the empirical fit by de Jager et al. (1988) does not provide the right values of the mass-loss rates. Furthermore,

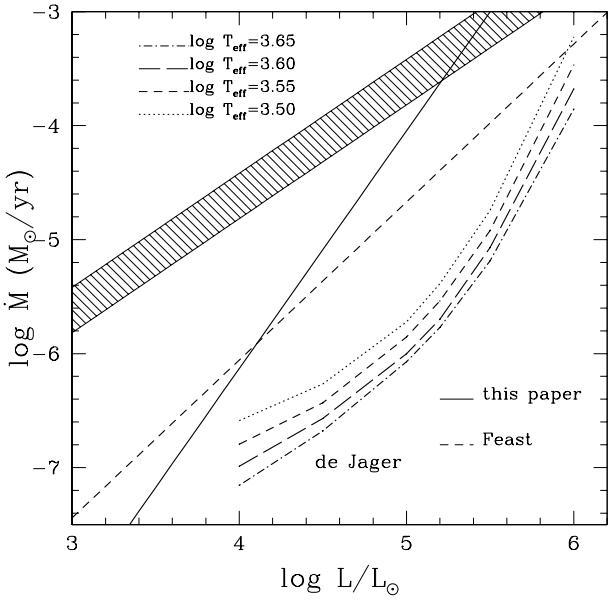

Fig. 7. Comparison of the mass-loss rates from different sources: the thin dotted, dashed, long dashed and dotted-dashed lines show the rates by de Jager et al.(1988) for different values of $\log T_{\rm eff}$. The heavy dashed line is the relation by Feast (1991), Eq. (12). The hatched area corresponds to the super-wind phase for the metallicity 0.008≤Z≤0.02 according to Eqs. (13) and (14) in the text. Finally, the heavy solid line shows the prescription for the mass-loss rate during the RSG stages we have adopted (see text for all details).

owing to the very large range of stellar parameters encompassed by the de Jager et al. (1988) relations, a loss of precision in particular areas of the HRD is always possible. Finally, we note that the super-wind mass-loss rate is about 5 times larger than the values derived by Feast (1991). As a conclusion, the current estimates for the mass-loss rates of RSG stars span the range 10^{-4} to $10^{-6} M_{\odot}$/yr.

Given these premises, we revisited the original determinations of the mass-loss rate for the stars upon which the Feast (1991) relation was derived.

One of the basic assumptions in the mass-loss estimates made by Jura & Kleinmann (1990) and Reid et al. (1990) is the value of the dust to gas ratio δ used to convert the mass-loss rate referred to the dust into the total mass-loss rate. By analogy with AGB stars, Jura (1986) adopted $\delta = 0.0045$ noticing, however, that a value as low as 0.001 could also be possible. Since the total rate of mass loss is expected to be inversely proportional to δ, the immediate consequence follows that the total mass-loss rates could be under-estimated by a a factor of 4.5.

If the high mass-loss rates in the RSG phase are ultimately driven by the transfer of the photon momentum to dust grains and gas, a tight relationship between the dust abundance and the velocity of the flow is expected. The problem has been studied by Habing et al. (1994), who confirmed that the terminal velocity $v_{\rm exp}$ of the gas flow in AGB stars depends rather strongly on the dust to gas ratio δ.

Along the same kind of arguments, Bressan et al. (1998) obtained the following expression for δ:

$$\delta \simeq 0.015 \times v^2_{\rm exp}[{\rm km/s}] \times \left(\frac{L}{L_\odot}\right)^{-0.7} \quad (15)$$

Inserting in this relation $v_{exp} = 15\,{\rm Km\ s^{-1}}$ and $\rm L = 10^4\,L_\odot$ (typical of AGB stars) one gets δ=0.005, which is nearly the value adopted by Jura & Kleinmann (1990) and Reid et al. (1990), thus confirming that this is the value suited to Mira and OH/IR stars.

In contrast, if we keep the velocity constant (though for periods above 500 days there are hints for a slightly increase with the period) and assume $\rm L = 10^5 L_\odot$ (typical of RSG star), we get $\delta \simeq 0.001$ indicating that at these high luminosities the mass-loss rates could have been under-estimated by a significant factor.

In order to include the effect of a systematic variation of the dust to gas ratio at increasing stellar luminosity on the mass-loss determination, as suggested by Eq. (15), we multiply the Feast (1991) relation by the factor $0.0045/\delta$ (i.e. we add the term $\log\,(0.0045/\delta)$ to Eq. (12) with δ given by Eq. (15)). The new mass-loss rate is given by

$$log(\dot{M}) = 2.1 \times log(\frac{L}{L_\odot}) - 14.5 \quad (16)$$

This law is shown by the heavy solid line in Fig. 7. The new relation is much steeper than the old one by Feast (1991). The mass-loss rate is about 2 times larger for a 15 $\rm M_\odot$ model and about 5 times larger for a 20 $\rm M_\odot$ model. The mass-loss rate gets the super-wind regime at about $\log(\rm L/L_\odot) \simeq 5.2$.

By analogy with AGB stars for which a relation between the mass-loss rate and the period has been proposed (Vassiliadis & Wood 1993), to fully legitimate the adoption of relation (16) in models of RSG stars, these latter should be tested against pulsational instability.

On the observational side, the majority of galactic RSG show luminosity variations from a few to several tenths of magnitude (depending also on the observed spectral region), thus suggesting that the RSG phase is most likely pulsationally unstable. Heger al. (1998) analyzed the stability of RSG models of 20 $\rm M_\odot$ and 15 $\rm M_\odot$ stars finding pulsational instability during the He-burning phase along the Hayashi line.

Although the whole subject deserves further studies by means of the ISO observations of winds of RSG stars, and a thorough investigation of the pulsational properties of RSG stars, for the aims of the present study we make use of the mass-loss rates predicted by relation (16) to check whether they can improve upon the situation encountered with the de Jager et al. (1988) prescription.

5. Models with the new mass-loss rate

In this section we describe the results for stars of initial masses 15 and 20 $\rm M_\odot$ and composition [Z=0.02, Y=0.28] and [Z=0.008, Y=0.25] that are calculated using the new mass-loss rate of Eq. (16) during the RSG stages, i.e. cooler than $\log \rm T_{eff} < 3.7$.

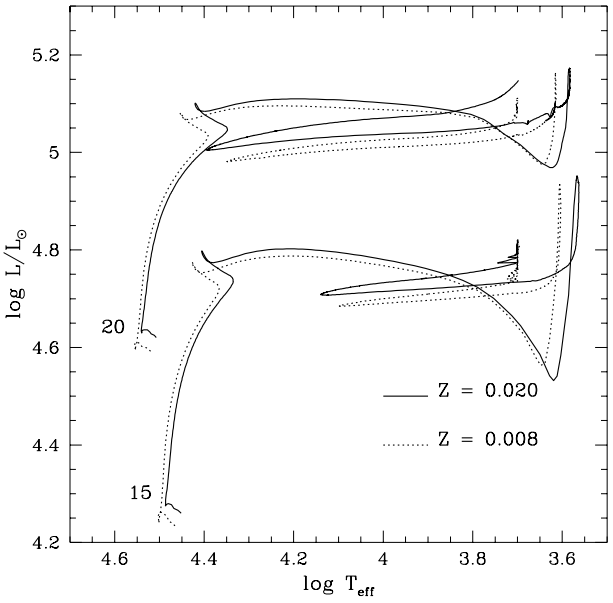

Fig. 8. Evolutionary path in the HRD of models calculated with the new diffusive scheme ($\alpha_1 = 0.015$, $\alpha_2 = 50$) and the mass-loss rate during the RSG stages according to relation (16). The solid lines are for [Z=0.02, Y=0.28], whereas the dotted lines are for [Z=0.008, Y=0.25]. The initial mass is indicated along the ZAMS.

The choice of the threshold temperature is based on these simple arguments: (i) RSG stars are found to be pulsationally unstable along the Hayashi line by Heger et al. (1998); (ii) the instability strip at the luminosity of about $\rm L = 10^5 L_\odot$ extends over the range $3.78 > \log \rm T_{eff} > 3.68$ and may even stretch to cooler temperature (Chiosi et al. 1993); (iii) mass loss during the red stages makes RSG stars even more prone to instability because of their high L/M ratios.

All the models are calculated with the same mixing parameters α_1 and α_2 as in the previous analysis with the de Jager et al. (1988) mass-loss rates, namely $\alpha_1 = 0.015$, and $\alpha_2 = 50$.

A summary of the main properties of the models we are going to discuss below is given in Table 3, which lists the model number (column 1), where 1 through 4 and 5 through 9 correspond to the core H-burning and He-burning, respectively; the age (column 2), the current mass (column 3), the logarithm of the luminosity (column 4); the logarithm of the effective temperature (column 5); the central content of hydrogen $\rm X_c$ or helium $\rm Y_c$ as appropriate (column 6); the fractionary mass $\rm Q_c$ of the convective core (column 7); the rate of mass loss (column 8), the surface abundance of hydrogen, helium, carbon, nitrogen, and oxygen (columns 9 through 13, respectively).

Fig. 8 shows the evolutionary tracks of the models computed with the new mass-loss rate in the RSG phase.

Looking at the 20 $\rm M_\odot$ star with solar composition and $\alpha_1 = 0.015$ as an example, it evolves as in case A until it reaches the Hayashi line with total mass of $M \approx 19$ $\rm M_\odot$. The vigorous mass loss ($\simeq 10^{-4} \rm M_\odot$/yr) in the low effective temperatures range peels off the star leaving a 8.6 $\rm M_\odot$ object which begins a very extended blue loop. The star spends $\approx 60\%$ of the He-

Table 3. Selected models of the 15 and 20 $M_\odot$ stars with the new diffusive scheme and the revised mass-loss rates during the RSG stage. The mixing parameters are $\alpha_1 = 0.015$ and $\alpha_2 = 50$. Age in years; Masses in solar units; Mass-loss rates in $M_\odot$/yr.

Mod	Age	M	L/L$_\odot$	T$_{eff}$	$X_c; Y_c$	Q_c	$\dot{M}$	X$_s$	Y$_s$	C$_s$	N$_s$	O$_s$
				20 M$_\odot$	Z=0.008		α_1=0.015	α_2=50				
1	0.00000E+00	20.00	4.597	4.553	0.738	0.6455	-8.171	7.42E-1	2.50E-1	1.37E-3	4.24E-4	3.85E-3
2	9.25539E+06	19.55	5.034	4.391	0.016	0.3917	-6.628	7.42E-1	2.50E-1	1.37E-3	4.24E-4	3.85E-3
3	9.37523E+06	19.52	5.074	4.448	0.000	0.3180	-6.632	7.42E-1	2.50E-1	1.37E-3	4.24E-4	3.85E-3
4	9.37665E+06	19.52	5.081	4.454	0.000	0.1094	-6.624	7.42E-1	2.50E-1	1.37E-3	4.24E-4	3.85E-3
5	9.38586E+06	19.52	5.095	4.240	0.992	0.0000	-6.387	7.42E-1	2.50E-1	1.37E-3	4.24E-4	3.85E-3
6	9.39248E+06	19.47	4.976	3.647	0.990	0.1611	-4.030	7.42E-1	2.50E-1	1.37E-3	4.24E-4	3.85E-3
7	9.39585E+06	18.94	5.164	3.616	0.987	0.1803	-3.656	6.63E-1	3.29E-1	7.91E-4	1.85E-3	2.95E-3
8	9.67735E+06	8.51	4.982	4.348	0.550	0.6442	-6.679	6.59E-1	3.33E-1	7.71E-4	1.91E-3	2.91E-3
9	1.01313E+07	8.10	5.115	3.701	0.000	0.0534	-6.170	6.59E-1	3.33E-1	7.34E-4	1.92E-3	2.91E-3
				15 M$_\odot$	Z=0.008		α_1=0.015	α_2=50				
1	0.00000E+00	15.00	4.243	4.501	0.738	0.6034	-9.193	7.42E-1	2.50E-1	1.37E-3	4.24E-4	3.85E-3
2	1.36222E+07	14.89	4.721	4.367	0.020	0.3509	-7.287	7.42E-1	2.50E-1	1.37E-3	4.24E-4	3.85E-3
3	1.38068E+07	14.88	4.770	4.424	0.000	0.2631	-7.283	7.42E-1	2.50E-1	1.37E-3	4.24E-4	3.85E-3
4	1.38078E+07	14.88	4.775	4.427	0.000	0.0542	-7.275	7.42E-1	2.50E-1	1.37E-3	4.24E-4	3.85E-3
5	1.38238E+07	14.88	4.784	4.127	0.992	0.0000	-6.902	7.42E-1	2.50E-1	1.37E-3	4.24E-4	3.85E-3
6	1.38295E+07	14.87	4.563	3.648	0.991	0.0800	-4.887	7.42E-1	2.50E-1	1.37E-3	4.24E-4	3.85E-3
7	1.38345E+07	14.58	4.934	3.606	0.987	0.1261	-4.140	6.84E-1	3.08E-1	8.32E-4	1.63E-3	3.14E-3
8	1.42990E+07	6.50	4.685	4.098	0.486	0.5358	-7.060	6.81E-1	3.11E-1	8.22E-4	1.67E-3	3.11E-3
9	1.48602E+07	5.81	4.807	3.696	0.000	0.2405	-4.407	6.81E-1	3.11E-1	8.14E-4	1.67E-3	3.11E-3
				20 M$_\odot$	Z=0.020		α_1=0.015	α_2=50				
1	0.00000E+00	20.00	4.631	4.540	0.696	0.6472	-7.811	7.00E-1	2.80E-1	3.43E-3	1.06E-3	9.63E-3
2	8.46560E+06	19.16	5.047	4.348	0.016	0.4153	-6.351	7.00E-1	2.80E-1	3.43E-3	1.06E-3	9.63E-3
3	8.58892E+06	19.10	5.091	4.413	0.000	0.3317	-6.344	7.00E-1	2.80E-1	3.43E-3	1.06E-3	9.63E-3
4	8.59017E+06	19.10	5.101	4.420	0.000	0.1142	-6.331	7.00E-1	2.80E-1	3.43E-3	1.06E-3	9.63E-3
5	8.59902E+06	19.09	5.108	4.111	0.981	0.0000	-6.137	7.00E-1	2.80E-1	3.43E-3	1.06E-3	9.63E-3
6	8.60352E+06	19.02	4.969	3.621	0.956	0.1350	-4.065	7.00E-1	2.80E-1	3.43E-3	1.06E-3	9.63E-3
7	8.61098E+06	17.56	5.172	3.584	0.947	0.1800	-3.639	6.17E-1	3.63E-1	2.00E-3	4.57E-3	7.40E-3
8	8.83758E+06	8.45	5.006	4.392	0.618	0.6690	-6.486	6.17E-1	3.63E-1	2.00E-3	4.57E-3	7.40E-3
9	9.32923E+06	8.08	5.191	3.783	0.000	0.4690	-5.943	4.95E-1	4.86E-1	8.11E-5	9.57E-3	4.29E-3
				15 M$_\odot$	Z=0.020		α_1=0.015	α_2=50				
1	0.00000E+00	15.00	4.275	4.487	0.697	0.5941	-8.786	7.00E-1	2.80E-1	3.43E-3	1.06E-3	9.63E-3
2	1.26136E+07	14.78	4.738	4.335	0.017	0.3666	-6.993	7.00E-1	2.80E-1	3.43E-3	1.06E-3	9.63E-3
3	1.27827E+07	14.76	4.791	4.401	0.000	0.2733	-6.985	7.00E-1	2.80E-1	3.43E-3	1.06E-3	9.63E-3
4	1.27839E+07	14.76	4.798	4.405	0.000	0.0451	-6.972	7.00E-1	2.80E-1	3.43E-3	1.06E-3	9.63E-3
5	1.27986E+07	14.76	4.783	4.016	0.981	0.0000	-6.656	7.00E-1	2.80E-1	3.43E-3	1.06E-3	9.63E-3
6	1.28026E+07	14.75	4.532	3.620	0.980	0.0565	-4.963	7.00E-1	2.80E-1	3.43E-3	1.06E-3	9.63E-3
7	1.28086E+07	14.36	4.952	3.567	0.977	0.1385	-4.101	6.42E-1	3.38E-1	2.18E-3	3.83E-3	7.99E-3
8	1.32390E+07	6.33	4.708	4.139	0.514	0.5659	-6.845	6.42E-1	3.38E-1	2.18E-3	3.84E-3	7.98E-3
9	1.38100E+07	5.92	4.821	3.699	0.000	0.1416	-4.378	6.42E-1	3.38E-1	2.16E-3	3.84E-3	7.98E-3

lifetime at $\log T_{\rm eff} > 4.2$. The surface H-abundance gets below X=0.62 already when the central He-content is $Y_c = 0.90$ and $\log T_{\rm eff} \leq$3.6. When Y_c drops below ≈ 0.2 the star goes back to the red side of the HRD. The surface H-abundance at the stage of central He-exhaustion is 0.5. Fig. 9 displays the evolutionary path in the HRD of the 20 $M_\odot$ models in a more detailed fashion. The central He-abundance and the fractional duration of the He-burning phase normalized to the whole He-burning lifetime are annotated along the evolutionary track.

How does the mass-loss rate vary in the course of evolution? and how does it compare with the observational data? This is shown in Fig. 10 where we plot the mass-loss rate (in $M_\odot$/yr) as a function of $\log T_{\rm eff}$ for the 20 $M_\odot$ star calculated with two laws for the mass-loss rate, i.e. de Jager et al. (1988) all over the evolutionary history (solid line) and the original relation (12)

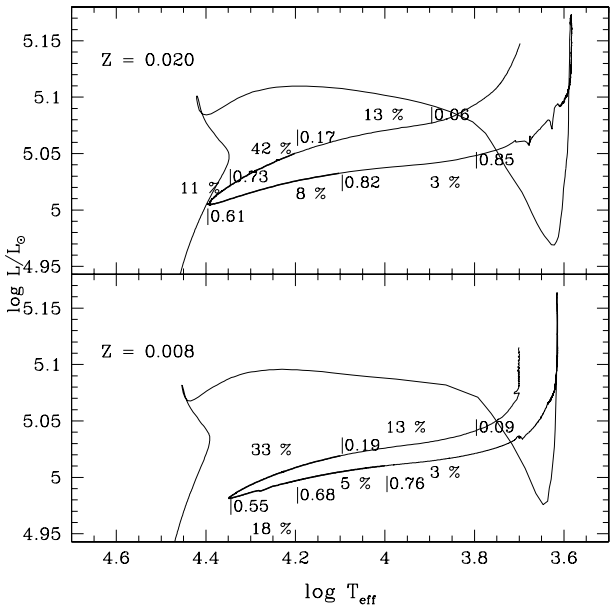

Fig. 9. Path in the HRD of the 20 $M_\odot$ star with the new diffusive scheme ($\alpha_1 = 0.015$, $\alpha_2 = 50$), and the new mass-loss rate during the RSG phase. The *top panel* is for the composition [Z=0.02, Y=0.28], whereas the *bottom panel* is for [Z=0.008, Y=0.25]. The numbers along the tracks indicate the central He-abundance and the fractional duration of the He-burning phase normalized to the whole He-burning lifetime

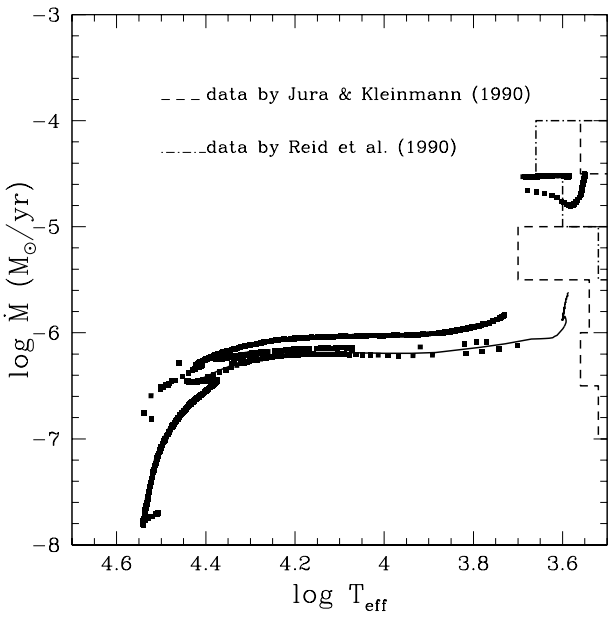

Fig. 10. Mass-loss rate as a function of $\log T_{\rm eff}$ for the 20 $M_\odot$ star with composition [Z=0.02, Y=0.28]. The solid line refers to the standard models with the mass-loss rate by de Jager et al. (1988). The squares correspond to the models with the mass-loss rates according to Feast (1991). All the models have the same mixing parameters, namely $\alpha_1 = 0.015$ and $\alpha_2 = 50$. The histogram on the right vertical axis shows the observational data by Jura & Kleinmann (1990) and Reid et al. (1990).

by Feast (1991) for the RSG stages (points). On the right vertical axis of Fig. 10 we plot the histogram of the observational data by Jura & Kleinmann (1990) for 21 red supergiants within 2.5 Kpc of the Sun (dashed line), and by Reid et al. (1990) for the RSG variables in LMC (dashed-dotted line). It is immediately evident that the de Jager et al. (1988) formulation severely under-estimates the mass-loss rates in the RSG phase. The mass-loss rates in the red predicted by Eq. (16) are even higher and cannot be directly compared with the observations without re-scaling these latter by the factor $0.0045/\delta$.

In summary, these models with much higher rate of mass loss during the RSG phase with respect to the standard values follow case A evolution and possess a blue loop extending into the main sequence band. Clearly these models are good candidates to solve the long lasting mystery of the missing BHG. This is shown in the panels of Fig. 11, which display the time (in years on a logarithmic scale) spent in various bins of effective temperature across the HRD. The dotted line is for the de Jager et al. (1988) prescription, whereas the solid line is for the new mass-loss rates in the RSG stages. It is soon evident that these models would predict a smooth distribution of stars across the HRD from the earliest to the latest spectral types.

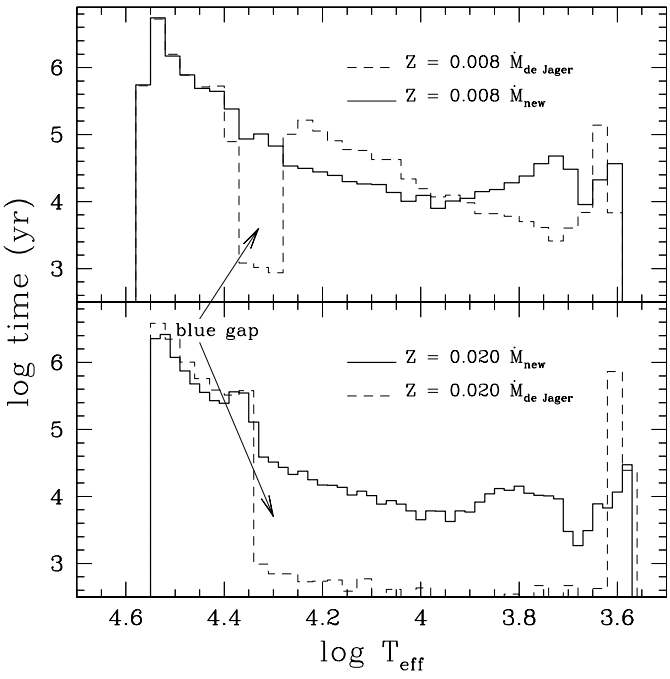

Fig. 11. Histogram of the elapsed time as a function of the effective temperature for the 20 $M_\odot$ stars with [Z=0.008, Y=0.250] (*upper panel*) and with [Z=0.020, Y=0.280] (*bottom panel*). The solid lines are for the mass-loss rate given by Eq. (16), whereas the dotted lines are for the Jager et al. (1988) prescription. All the models have the same mixing parameters, namely $\alpha_1 = 0.015$ and $\alpha_2 = 50$.

6. Tuning mixing under the new mass loss rates

Obvious objection to the analysis presented in the previous section is that we made use of the mixing parameters derived from models with the old mass-loss rates to calculate the models with the new prescription for the mass-loss rate and to infer from their properties the distribution of star in the HRD.

Table 4. Tuning mixing under the new mass-loss rate: the role of α_1.

Mod	Age	M	L/L$_\odot$	T$_{eff}$	$X_c; Y_c$	Q_c	$\dot{M}$	X$_s$	Y$_s$	C$_s$	N$_s$	O$_s$
				20 M$_\odot$	Z=0.008		α_1=0.009	α_2=50				
1	0.00000E+00	20.00	4.600	4.554	0.733	0.6455	-8.167	7.42E-1	2.50E-1	1.37E-3	4.24E-4	3.85E-3
2	8.59382E+06	19.64	4.990	4.414	0.022	0.3768	-6.753	7.42E-1	2.50E-1	1.37E-3	4.24E-4	3.85E-3
3	8.73670E+06	19.61	5.031	4.468	0.000	0.2853	-6.761	7.42E-1	2.50E-1	1.37E-3	4.24E-4	3.85E-3
4	8.73756E+06	19.61	5.037	4.472	0.000	0.0973	-6.756	7.42E-1	2.50E-1	1.37E-3	4.24E-4	3.85E-3
5	8.74945E+06	19.61	5.064	4.288	0.992	0.0000	-6.469	7.42E-1	2.50E-1	1.37E-3	4.24E-4	3.85E-3
6	8.80957E+06	19.58	5.129	4.029	0.889	0.1216	-6.302	7.42E-1	2.50E-1	1.37E-3	4.24E-4	3.85E-3
7	9.15326E+06	18.21	5.098	3.645	0.431	0.2673	-3.795	7.42E-1	2.50E-1	1.37E-3	4.24E-4	3.85E-3
8	9.15757E+06	17.50	5.108	3.635	0.424	0.2597	-3.775	7.42E-1	2.50E-1	1.36E-3	4.25E-4	3.85E-3
9	9.59578E+06	8.81	5.130	3.700	0.000	0.1731	-3.727	5.07E-1	4.85E-1	5.97E-5	4.00E-3	1.49E-3
				15 M$_\odot$	Z=0.008		α_1=0.009	α_2=50				
1	0.00000E+00	15.00	4.243	4.502	0.738	0.6034	-9.196	7.42E-1	2.50E-1	1.37E-3	4.24E-4	3.85E-3
2	1.27161E+07	14.92	4.668	4.385	0.025	0.3356	-7.454	7.42E-1	2.50E-1	1.37E-3	4.24E-4	3.85E-3
3	1.29255E+07	14.91	4.715	4.438	0.000	0.2259	-7.454	7.42E-1	2.50E-1	1.37E-3	4.24E-4	3.85E-3
4	1.29266E+07	14.91	4.718	4.441	0.000	0.0278	-7.450	7.42E-1	2.50E-1	1.37E-3	4.24E-4	3.85E-3
5	1.29474E+07	14.91	4.739	4.175	0.992	0.0000	-7.015	7.42E-1	2.50E-1	1.37E-3	4.24E-4	3.85E-3
6	1.29565E+07	14.90	4.503	3.643	0.951	0.0711	-5.043	7.42E-1	2.50E-1	1.37E-3	4.24E-4	3.85E-3
7	1.29607E+07	14.76	4.820	3.613	0.940	0.0887	-4.380	6.83E-1	3.09E-1	7.89E-4	1.66E-3	3.17E-3
8	1.34441E+07	6.20	4.597	3.708	0.470	0.4702	-6.861	6.83E-1	3.09E-1	7.89E-4	1.66E-3	3.17E-3
9	1.43566E+07	5.11	4.732	3.689	0.000	0.0979	-4.567	6.83E-1	3.09E-1	7.77E-4	1.66E-3	3.17E-3
				20 M$_\odot$	Z=0.020		α_1=0.009	α_2=50				
1	0.00000E+00	20.00	4.629	4.539	0.697	0.6505	-7.798	7.00E-1	2.80E-1	3.43E-3	1.06E-3	9.63E-3
2	8.01869E+06	19.31	5.008	4.378	0.019	0.3956	-6.463	7.00E-1	2.80E-1	3.43E-3	1.06E-3	9.63E-3
3	8.14918E+06	19.26	5.053	4.442	0.000	0.2864	-6.467	7.00E-1	2.80E-1	3.43E-3	1.06E-3	9.63E-3
4	8.14985E+06	19.26	5.058	4.446	0.000	0.0943	-6.461	7.00E-1	2.80E-1	3.43E-3	1.06E-3	9.63E-3
5	8.16100E+06	19.25	5.081	4.181	0.981	0.0000	-6.193	7.00E-1	2.80E-1	3.43E-3	1.06E-3	9.63E-3
6	8.16900E+06	19.14	4.964	3.622	0.924	0.1271	-4.072	7.00E-1	2.80E-1	3.43E-3	1.06E-3	9.63E-3
7	8.17460E+06	18.53	5.067	3.591	0.912	0.1416	-3.859	6.23E-1	3.56E-1	1.98E-3	4.37E-3	7.65E-3
8	8.64816E+06	7.91	5.020	4.307	0.272	0.6303	-6.363	4.99E-1	4.81E-1	2.63E-4	9.01E-3	4.63E-3
9	9.17945E+06	7.65	5.132	3.725	0.000	0.0704	-5.974	4.99E-1	4.81E-1	2.61E-4	9.01E-3	4.63E-3
				15 M$_\odot$	Z=0.020		α_1=0.009	α_2=50				
1	0.00000E+00	15.00	4.276	4.486	0.695	0.5941	-8.798	7.00E-1	2.80E-1	3.43E-3	1.06E-3	9.63E-3
2	1.16388E+07	14.83	4.688	4.356	0.022	0.3472	-7.148	7.00E-1	2.80E-1	3.43E-3	1.06E-3	9.63E-3
3	1.18280E+07	14.82	4.740	4.418	0.000	0.2414	-7.145	7.00E-1	2.80E-1	3.43E-3	1.06E-3	9.63E-3
4	1.18289E+07	14.82	4.745	4.421	0.000	0.0329	-7.136	7.00E-1	2.80E-1	3.43E-3	1.06E-3	9.63E-3
5	1.18478E+07	14.82	4.747	4.100	0.981	0.0000	-6.753	7.00E-1	2.80E-1	3.43E-3	1.06E-3	9.63E-3
6	1.18547E+07	14.81	4.419	3.626	0.978	0.0896	-5.137	7.00E-1	2.80E-1	3.43E-3	1.06E-3	9.63E-3
7	1.18599E+07	14.62	4.836	3.579	0.975	0.1178	-4.343	6.43E-1	3.37E-1	2.08E-3	3.87E-3	8.09E-3
8	1.25309E+07	5.84	4.629	3.754	0.292	0.5275	-6.689	6.43E-1	3.37E-1	2.08E-3	3.87E-3	8.09E-3
9	1.34179E+07	5.15	4.765	3.699	0.000	0.0000	-4.497	6.43E-1	3.37E-1	1.44E-3	4.31E-3	8.09E-3
				20 M$_\odot$	Z=0.008		α_1=0.021	α_2=50				
1	0.00000E+00	20.00	4.597	4.554	0.738	0.6472	-8.166	7.42E-1	2.50E-1	1.37E-3	4.24E-4	3.85E-3
2	9.78871E+06	19.44	5.077	4.361	0.015	0.4167	-6.502	7.42E-1	2.50E-1	1.37E-3	4.24E-4	3.85E-3
3	9.90819E+06	19.40	5.117	4.416	0.000	0.3541	-6.494	7.42E-1	2.50E-1	1.37E-3	4.24E-4	3.85E-3
4	9.90980E+06	19.40	5.128	4.424	0.000	0.1354	-6.481	7.42E-1	2.50E-1	1.37E-3	4.24E-4	3.85E-3
5	9.91701E+06	19.40	5.131	4.212	0.992	0.0000	-6.310	7.42E-1	2.50E-1	1.37E-3	4.24E-4	3.85E-3
6	9.92150E+06	19.29	5.028	3.653	0.991	0.1595	-3.981	7.42E-1	2.50E-1	1.37E-3	4.24E-4	3.85E-3
7	9.92499E+06	18.41	5.248	3.618	0.988	0.2141	-3.481	6.57E-1	3.35E-1	8.08E-4	1.91E-3	2.86E-3
8	1.01427E+07	8.95	5.051	4.551	0.639	0.7000	-6.911	6.56E-1	3.36E-1	8.03E-4	1.92E-3	2.85E-3
9	1.06363E+07	8.78	5.253	3.707	0.000	0.5455	-5.948	6.56E-1	3.36E-1	2.72E-4	2.48E-3	2.85E-3

Table 4. (continued)

Mod	Age	M	L/L$_\odot$	T$_{eff}$	$X_c; Y_c$	Q_c	$\dot{M}$	X$_s$	Y$_s$	C$_s$	N$_s$	O$_s$
				15 M$_\odot$	Z=0.008		α_1=0.021	α_2=50				
1	0.00000E+00	15.00	4.241	4.502	0.740	0.6090	-9.248	7.42E-1	2.50E-1	1.37E-3	4.24E-4	3.85E-3
2	1.46699E+07	14.85	4.777	4.343	0.016	0.3739	-7.113	7.42E-1	2.50E-1	1.37E-3	4.24E-4	3.85E-3
3	1.48331E+07	14.83	4.825	4.402	0.000	0.3002	-7.102	7.42E-1	2.50E-1	1.37E-3	4.24E-4	3.85E-3
4	1.48347E+07	14.83	4.834	4.407	0.000	0.0000	-7.088	7.42E-1	2.50E-1	1.37E-3	4.24E-4	3.85E-3
5	1.48469E+07	14.83	4.822	4.030	0.992	0.0000	-6.795	7.42E-1	2.50E-1	1.37E-3	4.24E-4	3.85E-3
6	1.48497E+07	14.82	4.635	3.645	0.992	0.0329	-4.835	7.42E-1	2.50E-1	1.37E-3	4.24E-4	3.85E-3
7	1.48596E+07	13.68	5.050	3.595	0.985	0.1704	-3.894	6.90E-1	3.02E-1	8.84E-4	1.57E-3	3.13E-3
8	1.52344E+07	6.34	4.769	4.634	0.546	0.6548	-7.966	6.90E-1	3.02E-1	8.40E-4	1.59E-3	3.13E-3
9	1.57929E+07	6.32	5.019	3.718	0.000	0.0001	-6.331	6.69E-1	3.22E-1	2.69E-4	2.41E-3	2.93E-3
				20 M$_\odot$	Z=0.020		α_1=0.021	α_2=50				
1	0.00000E+00	20.00	4.631	4.540	0.695	0.6505	-7.818	7.00E-1	2.80E-1	3.43E-3	1.06E-3	9.63E-3
2	9.00791E+06	18.94	5.089	4.307	0.010	0.4374	-6.232	7.00E-1	2.80E-1	3.43E-3	1.06E-3	9.63E-3
3	9.10291E+06	18.88	5.129	4.373	0.000	0.3724	-6.218	7.00E-1	2.80E-1	3.43E-3	1.06E-3	9.63E-3
4	9.10439E+06	18.88	5.143	4.382	0.000	0.1346	-6.196	7.00E-1	2.80E-1	3.43E-3	1.06E-3	9.63E-3
5	9.11181E+06	18.88	5.135	3.994	0.981	0.0024	-6.092	7.00E-1	2.80E-1	3.43E-3	1.06E-3	9.63E-3
6	9.11425E+06	18.81	5.023	3.632	0.980	0.1135	-3.958	7.00E-1	2.80E-1	3.43E-3	1.06E-3	9.63E-3
7	9.12481E+06	15.42	5.265	3.583	0.971	0.2861	-3.446	6.14E-1	3.66E-1	2.08E-3	4.59E-3	7.24E-3
8	9.33104E+06	8.92	5.066	4.784	0.661	0.7159	-7.658	4.76E-1	5.04E-1	2.53E-4	9.78E-3	3.74E-3
9	9.82381E+06	8.87	5.272	3.806	0.000	0.5370	-5.818	4.72E-1	5.08E-1	9.90E-5	1.01E-2	3.65E-3
				15 M$_\odot$	Z=0.020		α_1=0.021	α_2=50				
1	0.00000E+00	15.00	4.275	4.486	0.698	0.5941	-8.834	7.00E-1	2.80E-1	3.43E-3	1.06E-3	9.63E-3
2	1.34604E+07	14.71	4.788	4.307	0.016	0.3891	-6.837	7.00E-1	2.80E-1	3.43E-3	1.06E-3	9.63E-3
3	1.36307E+07	14.68	4.838	4.372	0.000	0.3299	-6.824	7.00E-1	2.80E-1	3.43E-3	1.06E-3	9.63E-3
4	1.36327E+07	14.68	4.853	4.381	0.000	0.0550	-6.798	7.00E-1	2.80E-1	3.43E-3	1.06E-3	9.63E-3
5	1.36441E+07	14.68	4.823	3.923	0.981	0.0000	-6.558	7.00E-1	2.80E-1	3.43E-3	1.06E-3	9.63E-3
6	1.36463E+07	14.66	4.639	3.625	0.980	0.0159	-4.790	7.00E-1	2.80E-1	3.43E-3	1.06E-3	9.63E-3
7	1.36564E+07	13.52	5.051	3.554	0.975	0.1816	-3.892	6.44E-1	3.36E-1	2.31E-3	3.69E-3	7.95E-3
8	1.39739E+07	6.35	4.751	4.638	0.619	0.6544	-7.845	6.44E-1	3.36E-1	2.21E-3	3.72E-3	7.95E-3
9	1.45868E+07	6.31	4.988	3.713	0.000	0.3692	-6.171	6.44E-1	3.36E-1	2.74E-4	6.10E-3	7.95E-3

Since mixing concurs to determine the properties of the stellar models, the question arises whether with the new mass-loss rates the mixing parameters remain the same.

In order to answer the above question, we have repeated the kind of analysis presented in Sect. 3, using the mass loss rate of relation 16 for the red supergiant stages of the 15 and 20 M$_\odot$ stars and varying the parameters α_1 and α_2. Many numerical experiments have been performed at varying α_1 and α_2, which ultimately confirm the scenario emerging from the previous analysis. For the sake of simplicity we present here only a few selected cases yielding results that are best suited to interpret the observational HRD.

Variation of α_1. Two sets of models are considered, i.e. those with $\alpha_1 = 0.009$ and $\alpha_1 = 0.021$ which bracket the value of 0.015 indicated by the previous analysis. The results are presented in Table 4 for $\alpha_1 = 0.009$ and 0.021, respectively. In both cases $\alpha_2 = 50$.

The results obey the general scheme already outlined in Sect. 3: for $\alpha_1 = 0.021$ extended loops are possible, whereas for $\alpha_1 = 0.009$ the situation is more intrigued: models of 15 M$_\odot$ remain for the whole He-burning phase at low effective temperatures with sporadic excursions to the blue of very short duration. The model of 20 M$_\odot$ and Z=0.008 behaves as a case B and is affected by the new mass-loss only at helium exhaustion, while the one with solar composition performs an extended loop.

Variation of α_2. Limited to the case of the 20 M$_\odot$ we now vary α_2 in models with $\alpha_1 = 0.015$ and explore the window at $\alpha_1 = 0.009$ and $\alpha_2 = 500$, as suggested by Table 1. The results are shown in Table 5. In the cases with $\alpha_1 = 0.015$ the loops get wider and wider at increasing α_2. In the other case, corresponding to a possible case A with low α_1, the Z=0.008 model perform a very extended blue loop, while the Z=0.020 model ends up as a WR star. Therefore with the new mass-loss rate models with $\alpha_1 = 0.009$ are only marginally acceptable, limited to high values of α_2 ($\alpha_2 \geq 500$); models with lower α_1 can be ruled out.

Full exploration of the parameters α_1, α_2 and $\dot{M}_{red}$ is a cumbersome affair not worth being pursued as it would depend

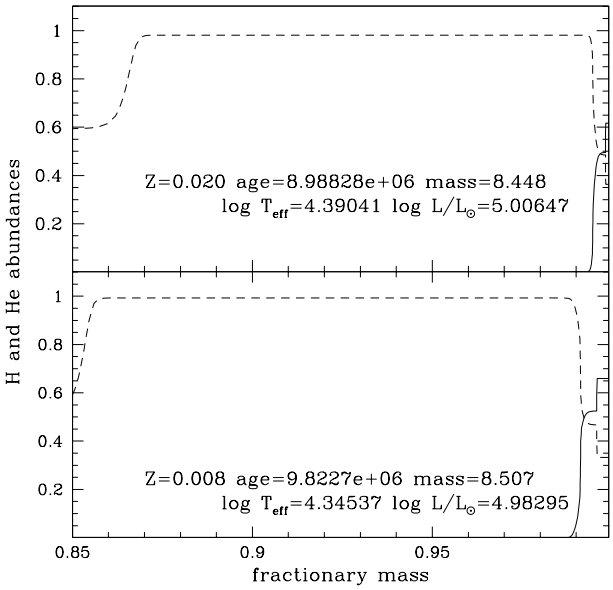

Fig. 12. The internal H- and He-profiles (continuous and dashed lines, respectively) of the 20 $M_\odot$ models with [Z=0.020, Y=0.28] (*upper panel*) and [Z=0.008, Y=0.25] (*bottom panel*) during the blue loop. Masses are in solar units.

on the particular recipes for mixing and mass loss rates in usage that are far from being fully settled down.

Despite this limitation, a number of useful hints can be derived from the above analysis which allow us to qualitatively understand the different role played by the three parameters.

(i) α_1 determines the size of the overshoot region from the central core and mixing over there, affects the luminosity and lifetime of the core H-burning phase, and to a certain extent decides which of the three main schemes (A, B, and C) is followed by the star during its core He-burning stages.

(ii) α_2 regulates mixing in the intermediate convective shell, governs the initial and final luminosity of the star along the Hayashi line and therefore greatly affects the rate of mass loss along it. Together with the duration of the red phase (in turn affected by α_1) and the specific assumption for the dependence of mass-loss rate on basic stellar parameters, to a certain extent α_2 determines how much mass can be lost during the RSG stages.

(iii) At given α_1 and α_2, mass loss along the Hayashi line decides whether a star can perform extended loops. High mass-loss rates in the RSG stages favour of course such an occurrence.

(iv) Finally, small details of the loop phase are once more governed by α_2.

Under a given assumption for the mass-loss rate across the HRD (in the red in particular), α_1 and α_2 have somewhat contrasting effects. The final interplay among the various factors determines the path of the star in the HRD.

7. Internal mixing or mass loss?

The aim of this section is to understand which between mixing and mass loss is the key factor determining the kind of models that apparently succeed to account for the distribution of massive stars in the HRD.

The internal structure of all the models during the blue supergiant phase (Fig. 12) is very similar. The helium core is surrounded by a thin hydrogen envelope, whose fractionary mass is about 1%–5% of the current total mass. This characteristic seems an essential condition in order to get core He-burning models in the effective temperature range $4.5 \geq \log T_{\rm eff} \geq 4.2$. Clearly the high mass-loss rates we have adopted strip the models of their envelopes and provide a simple explanation of the blue extension of the loop.

We have already seen that internal mixing determines the evolutionary pattern in the HRD, i.e. which of the three avenues (case A, B and C) is followed by a star. Furthermore, with the standard and new mass-loss rates during the RSG stages, we have derived the values of α_1 and α_2 yielding the widest loops across the HRD.

In this context we remark that case B (slow redward evolution) can be almost certainly excluded because the stars would not be able to live as RSG long enough to undergo significant mass loss over there and perform short-lived loops at the end of core He-burning. This is particularly true for low metallicities for which evolution without overshoot leads more easily to the case B scheme.

Case A models with the new adopted mass-loss rates during the RSG phase are best suited to performing extended loops, and explaining the many stars in the BHG, and the enhancement in the surface abundances of He and CNO elements seen in many of these objects. They are also best suited to interpreting the stellar content of individual clusters, NGC 330 of the SMC as a prototype, in which several studies have revealed the presence of a significant number of blue supergiant stars near the main sequence band (Caloi et al. 1993; Vallenari et al. 1994; Chiosi et al. 1995), which cannot be explained by other types of models.

Whether case C models (whole core He-burning as RSG, and fully mixed overshoot regions) are able to perform extended blue loops is a matter of fine tuning the new mass-loss rate which is beyond the aim of the present paper.

Finally to fully understand the role of the internal mixing, in particular whether it would be possible to recover at least part of the results obtained with the much higher mass-loss rates in the red, we have performed a series of numerical experiments on the evolutionary sequence of the case-A 20 $M_\odot$ star ($\alpha_1 = 0.015$; $\alpha_2 \simeq 50$) calculated with the de Jager et al. (1988) mass-loss rates all over the HRD. We anticipate that similar results can be obtained using the 20 $M_\odot$ star calculated with the fully mixed overshoot scheme in the convective core and the Schwarzschild condition for the instability in the intermediate convective shell. These latter experiments are not shown here for the sake of brevity.

The 20 $M_\odot$ star in usage here belongs to case-A evolution and when it leaves the RSG phase the envelope mass is about about 12 $M_\odot$. We take the bluest model in the loop as the reference model on which the experiments are performed. Starting from this, we calculate several sequences of equilibrium models (without the gravitational energy source, see Lauterborn et

Table 5. Tuning mixing under the new mass-loss rate: the role of α_2.

Mod	Age	M	L/L$_\odot$	T$_{eff}$	$X_c; Y_c$	Q_c	$\dot{M}$	X$_s$	Y$_s$	C$_s$	N$_s$	O$_s$
				20 M$_\odot$	Z=0.020		α_1=0.015	α_2=1				
1	0.00000E+00	20.00	4.631	4.540	0.696	0.6472	-7.811	7.00E-1	2.80E-1	3.43E-3	1.06E-3	9.63E-3
2	8.45758E+06	19.16	5.046	4.348	0.017	0.4153	-6.353	7.00E-1	2.80E-1	3.43E-3	1.06E-3	9.63E-3
3	8.58706E+06	19.10	5.081	4.404	0.000	0.3682	-6.350	7.00E-1	2.80E-1	3.43E-3	1.06E-3	9.63E-3
4	8.58992E+06	19.10	5.099	4.418	0.000	0.1142	-6.343	7.00E-1	2.80E-1	3.43E-3	1.06E-3	9.63E-3
5	8.59916E+06	19.09	5.130	4.153	0.981	0.0000	-6.106	7.00E-1	2.80E-1	3.43E-3	1.06E-3	9.63E-3
6	8.60605E+06	18.96	5.104	3.659	0.679	0.2710	-3.774	7.00E-1	2.80E-1	3.43E-3	1.06E-3	9.63E-3
7	8.61213E+06	17.79	5.149	3.617	0.675	0.2803	-3.684	7.00E-1	2.80E-1	3.42E-3	1.06E-3	9.63E-3
8	8.96031E+06	9.13	5.123	3.776	0.289	0.6103	-6.042	4.77E-1	5.03E-1	1.63E-4	9.32E-3	4.44E-3
9	9.21275E+06	8.22	5.199	3.729	0.000	0.0000	-5.870	4.77E-1	5.03E-1	1.42E-4	9.35E-3	4.44E-3
				20 M$_\odot$	Z=0.020		α_1=0.015	α_2=50				
1	0.00000E+00	20.00	4.631	4.540	0.696	0.6472	-7.811	7.00E-1	2.80E-1	3.43E-3	1.06E-3	9.63E-3
2	8.46560E+06	19.16	5.047	4.348	0.016	0.4153	-6.351	7.00E-1	2.80E-1	3.43E-3	1.06E-3	9.63E-3
3	8.58892E+06	19.10	5.091	4.413	0.000	0.3317	-6.344	7.00E-1	2.80E-1	3.43E-3	1.06E-3	9.63E-3
4	8.59017E+06	19.10	5.101	4.420	0.000	0.1142	-6.331	7.00E-1	2.80E-1	3.43E-3	1.06E-3	9.63E-3
5	8.59902E+06	19.09	5.108	4.111	0.981	0.0000	-6.137	7.00E-1	2.80E-1	3.43E-3	1.06E-3	9.63E-3
6	8.60352E+06	19.02	4.969	3.621	0.956	0.1350	-4.065	7.00E-1	2.80E-1	3.43E-3	1.06E-3	9.63E-3
7	8.61098E+06	17.56	5.172	3.584	0.947	0.1800	-3.639	6.17E-1	3.63E-1	2.00E-3	4.57E-3	7.40E-3
8	8.83758E+06	8.45	5.006	4.392	0.618	0.6690	-6.486	6.17E-1	3.63E-1	2.00E-3	4.57E-3	7.40E-3
9	9.32923E+06	8.08	5.191	3.783	0.000	0.4690	-5.943	4.95E-1	4.86E-1	8.11E-5	9.57E-3	4.29E-3
				20 M$_\odot$	Z=0.020		α_1=0.015	α_2=100				
1	0.00000E+00	20.00	4.632	4.540	0.694	0.6472	-7.812	7.00E-1	2.80E-1	3.43E-3	1.06E-3	9.63E-3
2	8.44177E+06	19.15	5.048	4.348	0.014	0.4141	-6.349	7.00E-1	2.80E-1	3.43E-3	1.06E-3	9.63E-3
3	8.54885E+06	19.10	5.077	4.399	0.000	0.3785	-6.350	7.00E-1	2.80E-1	3.43E-3	1.06E-3	9.63E-3
4	8.55330E+06	19.10	5.098	4.419	0.000	0.1071	-6.346	7.00E-1	2.80E-1	3.43E-3	1.06E-3	9.63E-3
5	8.56186E+06	19.10	5.110	4.149	0.981	0.0000	-6.148	7.00E-1	2.80E-1	3.43E-3	1.06E-3	9.63E-3
6	8.56662E+06	19.05	4.970	3.622	0.980	0.1937	-4.032	7.00E-1	2.80E-1	3.43E-3	1.06E-3	9.63E-3
7	8.57018E+06	18.51	5.183	3.582	0.979	0.2558	-3.643	6.28E-1	3.52E-1	2.16E-3	4.12E-3	7.67E-3
8	8.84801E+06	8.33	5.014	4.455	0.588	0.6789	-6.573	6.18E-1	3.62E-1	2.05E-3	4.47E-3	7.43E-3
9	9.33567E+06	8.17	5.222	3.751	0.000	0.5758	-5.872	4.66E-1	5.14E-1	1.99E-4	9.91E-3	3.69E-3
				20 M$_\odot$	Z=0.020		α_1=0.009	α_2=500				
1	0.00000E+00	20.00	4.630	4.540	0.696	0.6505	-7.800	7.00E-1	2.80E-1	3.43E-3	1.06E-3	9.63E-3
2	7.96446E+06	19.31	5.008	4.378	0.019	0.3971	-6.464	7.00E-1	2.80E-1	3.43E-3	1.06E-3	9.63E-3
3	8.09318E+06	19.26	5.052	4.440	0.000	0.2974	-6.466	7.00E-1	2.80E-1	3.43E-3	1.06E-3	9.63E-3
4	8.09423E+06	19.26	5.058	4.445	0.000	0.0895	-6.457	7.00E-1	2.80E-1	3.43E-3	1.06E-3	9.63E-3
5	8.10584E+06	19.26	5.063	4.128	0.981	0.0000	-6.214	7.00E-1	2.80E-1	3.43E-3	1.06E-3	9.63E-3
6	8.11098E+06	19.24	4.834	3.622	0.979	0.1280	-4.244	7.00E-1	2.80E-1	3.43E-3	1.06E-3	9.63E-3
7	8.11900E+06	17.91	5.131	3.580	0.974	0.1766	-3.725	6.38E-1	3.42E-1	2.10E-3	3.95E-3	7.96E-3
8	8.32346E+06	7.17	4.852	4.946	0.681	0.6917	-4.389	2.61E-1	7.20E-1	1.60E-4	1.26E-2	8.07E-4
9	8.94131E+06	3.92	4.549	5.099	0.000	0.0000	-5.606	0.00E+0	6.39E-1	3.20E-1	6.83E-8	1.51E-2
				20 M$_\odot$	Z=0.008		α_1=0.009	α_2=500				
1	0.00000E+00	20.00	4.600	4.554	0.733	0.6455	-8.167	7.42E-1	2.50E-1	1.37E-3	4.24E-4	3.85E-3
2	8.60637E+06	19.64	4.992	4.415	0.019	0.3750	-6.751	7.42E-1	2.50E-1	1.37E-3	4.24E-4	3.85E-3
3	8.72833E+06	19.61	5.021	4.459	0.000	0.3247	-6.762	7.42E-1	2.50E-1	1.37E-3	4.24E-4	3.85E-3
4	8.73325E+06	19.61	5.028	4.469	0.000	0.0452	-6.765	7.42E-1	2.50E-1	1.37E-3	4.24E-4	3.85E-3
5	8.74399E+06	19.61	5.059	4.233	0.992	0.0000	-6.449	7.42E-1	2.50E-1	1.37E-3	4.24E-4	3.85E-3
6	8.75313E+06	19.56	4.908	3.641	0.988	0.1651	-4.181	7.42E-1	2.50E-1	1.37E-3	4.24E-4	3.85E-3
7	8.75875E+06	18.80	5.096	3.616	0.982	0.2207	-3.797	6.97E-1	2.95E-1	8.53E-4	1.47E-3	3.30E-3
8	9.57743E+06	8.32	5.078	4.464	0.175	0.6545	-6.618	4.85E-1	5.07E-1	1.04E-4	4.14E-3	1.26E-3
9	9.98633E+06	8.18	5.206	3.745	0.000	0.5789	-6.092	4.75E-1	5.17E-1	9.96E-5	4.21E-3	1.19E-3

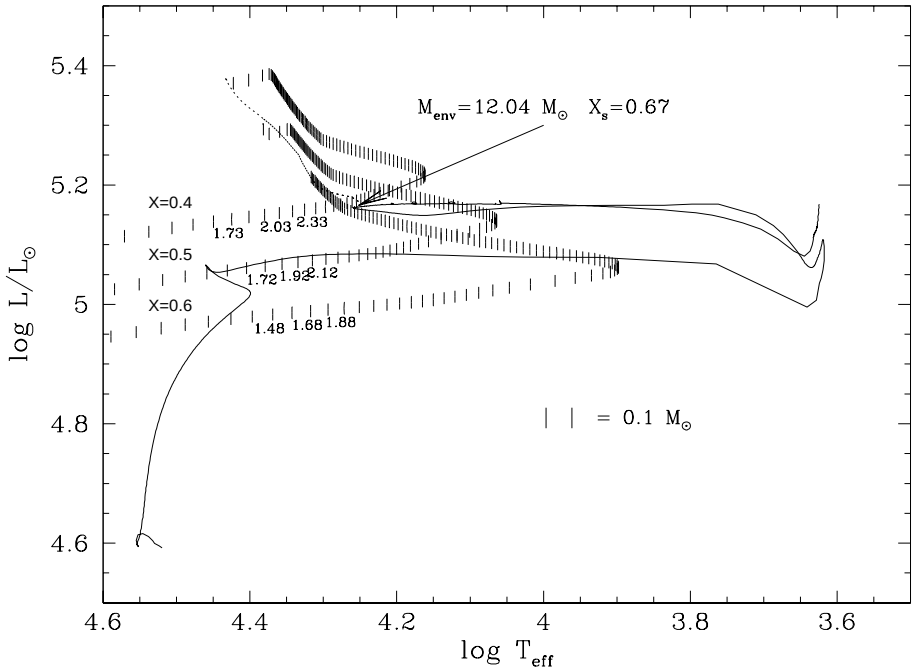

Fig. 13. Equilibrium models at varying surface abundance of hydrogen and envelope mass. The solid line is the sequence of $20M_\odot$ model with [Z=0.008, Y=0.25] computed with our diffusive scheme and de Jager et al. (1988) mass-loss rate. Starting from the bluest model of the loop, the envelope H-abundance has been lowered to 0.6, 0.5 and 0.4 (the models evolve along the dotted line). At these selected values, sequences of varying envelope mass have been constructed. The vertical bars mark decrements of 0.1 $M_\odot$ in the envelope mass. The numbers along the three sequences indicate the envelope mass of the models.

al. 1971), which have different surface hydrogen abundance and envelope mass. The adopted surface abundances of hydrogen are X=0.6, 0.5, and 0.4. The envelope mass is decreased in steps of 0.1 $M_\odot$. All these evolutionary sequences are shown in Fig. 13.

First we artificially decrease the envelope abundance to the selected value. These models follow the dotted line in Fig 13. Once the selected surface abundance has been reached, we decrease the envelope mass. Each vertical bar in Fig. 13 marks a decrement of 0.1 $M_\odot$.

Decreasing the surface H-abundance makes the models hotter and more luminous, because of the higher mean molecular weight. They move toward a pure helium sequence. For instance, the starting models with X=0.5 and 0.4 even reach the main sequence band of more massive stars.

In order to reach this configuration, an evolutionary scheme is required, in which an additional amount of about $2M_\odot$ (for X=0.5) or $3M_\odot$ (for X=0.4) of hydrogen is burned and mixed to the surface during or before the RSG phase. This could happen with a larger overshoot distance during the main sequence phase (in order to increase the mass of the burned hydrogen) followed by a deeper penetration of the convective envelope during the RSG phase. However, this would imply that envelope convection should be able to penetrate very deep inside a star (up to several pressure scale heights). Unfortunately, the models computed by Alongi et al. (1991) with envelopes whose overshooting distance is 0.7 H_P, can actually erode and mix only a tiny fraction of the inner He-rich core. Other mechanisms, such as rotationally induced mixing, have been investigated by several authors (see Eryurt et al. 1994, Talon et al. 1997). None of these models, however, agrees with the kind of evolution suggested by the observational data.

The equilibrium sequences of decreasing envelope mass shown in Fig. 13 demonstrate that envelope masses in the range 1 to 2 $M_\odot$ are required in order to populate the high effective temperature region between the main sequence band and the loop. Clearly, the higher the H-surface abundance, the lower is the envelope mass at a given effective temperature.

Therefore, unless a still unknown mixing mechanism operates to lower the H-abundance in the envelope below 0.5, the only possible way to populate the BHG is to get envelope masses below 2 $M_\odot$. In this case internal mixing may help, but not cause, the blueward extension of the model.

It is worth noticing that large mass-loss rates in the red have already been suggested, see Chiosi et al. (1978) who adopted a similar scheme. They made use of radiation-driven wind formulation during the main sequence phase, and adopted a mass-loss rate proportional to the acoustic flux in the RSG phase. A mass-loss rate as high as few $10^{-4}M_\odot$/yr was obtained for their $20M_\odot$ model during the RSG phase. Unfortunately, due to numerical difficulties their sequence was not able to evolve blueward of $\log T_{\rm eff} \simeq 4.2$, while the models were still performing the blue loop, so that it was not possible to evaluate the maximum extension toward the blue. Because of the high mass-loss rate applied during the RSG phase, their $20M_\odot$ model can be considered as the ancestor of the evolutionary scheme suggested in this study.

8. Discussion and conclusions

In this paper we have revisited the evolution of massive stars in the mass range 15 to 30 $M_\odot$, which roughly corresponds to the area of the HRD in which both blue and red supergiant stars coexist. Extant observational data provide hints to understand some important mechanisms that are at the base of the evolution of this class of stars. Despite their relatively simple internal structure during both core H- and He-burning, all the models computed in the past fail in reproducing some well established observational facts. First, the so called "Blue Hertzsprung

Gap", the region of the HRD near the main sequence band which is well populated almost independently from the environment (Solar Vicinity, LMC, SMC), and, on the contrary, is crossed by the models in a Kelvin-Helmholtz time-scale. Second, blue supergiant stars in this area of the HRD are also He-enriched and show CNO abundance characteristic of the first dredge-up episode, indicating that they underwent the RSG phase and are now burning helium in the center while performing a very extended blue loop.

To understand the reason of the failure of current models with respect to those observational constraints, we re-examined the effects of both internal mixing and mass loss by stellar winds (during the red stages in particular).

Mixing. Utilizing suggestions from recent hydro-dynamical calculations, we model internal mixing as a turbulent diffusive process and account for the exponential decay of the convective velocities outside the classical Schwarzschild border. The characteristic decay scale is parameterized by a suitable fraction of the pressure scale height (α_1).

As far as the intermediate convective zone is concerned, we follow Langer et al. (1983, 1985) who included a time dependent mixing process. The efficiency of this intermediate convective mixing is parameterized by α_2.

By suitably choosing the parameters α_1 and α_2 we can reproduce a wide range of mixing topologies, from the standard semiconvective one to the full overshoot scheme.

We performed an extensive analysis to determine the combination of the parameters α_1 and α_2 yielding the most extended loop for a typical 20$M_\odot$ star with LMC composition and mass loss by stellar wind according to the de Jager et al. (1988) relationships.

The test experiments for the parameter selection and the corresponding evolutionary models show that internal mixing alone cannot be responsible of the observed star distribution in the region between the main sequence band and the blue side of the loop.

Despite the new prescription of internal mixing, these models are much similar to others in literature and share many of their weak points. In brief, for the adopted values of α_1 and α_2, the 20 $M_\odot$ star with LMC composition is able to perform extended loops (case A), whereas the same star but with solar composition has the whole core He-burning phase as a RSG (case C). Finally, all these models predict the BHG in the HRD.

Mass loss. Examining the causes of the failure, we find that the mass-loss rates in the RSG phase by de Jager et al. (1988) actually under-estimate the observational values by a large factor.

We start from the mass-loss rates for red supergiants given by Feast (1991) based on the data by Jura & Kleinmann (1990) and Reid et al. (1990). These are about an order of magnitude larger than the previous ones. However, the close inspection of these data show that even the rates quoted by Feast (1991) could be systematically under-estimated with respect to reality because they were derived assuming the dust to gas ratio $\delta = 0.0045$ holding for the physical conditions in the expanding layers of AGB stars. By suitably correcting for the different physical conditions of red supergiant stars (different dust to gas ratio), we propose and make use of a new relationships for the mass loss rate as a function of the luminosity which runs steeper than that of Feast (1991). At the luminosity of a typical 20 $M_\odot$ star the new mass loss rate is about a factor of 5 and 15 higher than predicted by Feast (1991) and de Jager et al. (1988), respectively. We remind the reader that the new mass-loss rates are below the super-wind regime, at least in the luminosity range of interest here.

Models in the mass range 15- 20$M_\odot$ stars with solar and LMC composition develop extended loops across the HRD. The same is true for models of the same mass but the chemical composition typical of the SMC (Z=0.004). They are not described here for the sake of brevity.

Equilibrium models. Finally, to clarify the combined role of mass-loss and internal mixing we computed static equilibrium configurations at varying surface hydrogen abundance and envelope mass. A 20$M_\odot$ star with standard mass-loss rates in the red, while performing the loop, has a H-rich envelope of about 12 $M_\odot$. If the H-abundance in the envelope of this star is let decrease by some mixing mechanism down to 0.4, then the star would shift toward higher luminosity and hit the main sequence. However, arguments are given to claim that an evolutionary scenario yielding this kind of stellar structure does not exist and most likely is even not possible.

In contrast, static models with conventional mixing but envelope mass below 2$M_\odot$ populate the blue gap, naturally suggesting that mass-loss (in the red) is the leading parameter of the problem. For a given relationship between the mass-loss rate and the luminosity, the blue loops are more extended at increasing luminosity of the models during the RSG stages (which in turn depends on α_1 and/or α_2) or increasing duration of the phase in which the new mass loss rate is active (higher threshold effective temperature).

Therefore, we suggest that a thorough, both observational and theoretical revision of the mass-loss rates during the RSG phase is urgently needed.

A word of caution. The extension of the overshoot regions surrounding the fully convective core stands on the Grossman (1996) modeling of convection and mixing over there is treated with the diffusion formalism. The diffusion coefficient decays exponentially with radial distance from the border of the Schwarzschild core with the typical scale-length $\alpha_1 \times H_P$. The original formulation predicted $\alpha_1 \simeq 0.5$, whereas our analysis, ultimately based on the comparison between model results and observations, hints much lower values, i.e. in the range $0.01 \leq \alpha_1 \leq 0.02$ which roughly corresponds to a overshooting distance of about $0.15 \times H_P$. This result somewhat weakens the Grossman (1996) modeling of convection.

Another point to be mentioned concerns the diffusion coefficient in the intermediate convective shell. In this region we made use of the Langer et al. (1983, 1985) suggestion that the

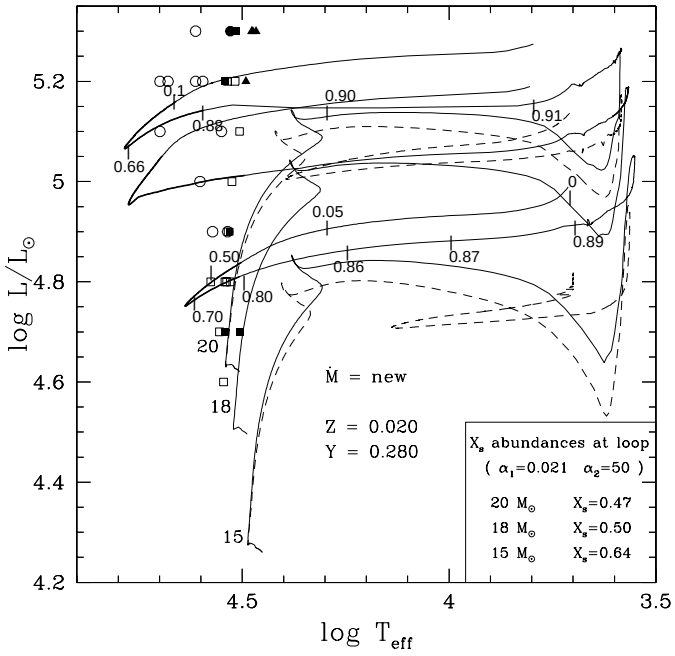

Fig. 14. HRD of stars with solar composition [Z=0.02, Y=0.28] and mass in the range 15–20 $M_\odot$ calculated with the new diffusive scheme and the revised mass-loss rates during the RSG stages. Solid lines correspond to models calculated with $\alpha_1 = 0.021$, while dashed lines to those with $\alpha_1 = 0.015$. The slow stages of the core He-burning are indicated by heavier lines. Finally, the filled and open circles show the WR stars of Hamann et al. (1993). The meaning of the symbols is the same as in Fig. 6. Note the new channel for the formation of the low-luminosity WR stars (see the text for more details).

thermal time scale drives the diffusion coefficient and mixing over there. We find that acceptable models are possible only for large values of α_2 (50 to 100), which implies a diffusive time scale much longer than the mere thermal time scale. This result agree with that by Langer et al. (1983, 1985).

WR stars. Finally, we like to draw some remarks on the use of these models to interpret the observational properties of WR stars. We start noticing that soon after leaving the RSG region, the surface H-abundance of the 15 and 20 $M_\odot$ models can be as low as 0.47 (see for instance the case with $\alpha_1 = 0.021$ and $\alpha_2 = 50$), i.e. close to the value of 0.40 assumed by Maeder (1990) to mark the transition from O-type to WNL stars. Furthermore these values are consistent, within the uncertainty limits, with the ones observed by Hamann et al. (1993) in some WNL stars. Fig. 14 shows the path in the HRD of the 15, 18 and 20 $M_\odot$ stars with solar composition and $\alpha_1 = 0.021$ and the 15 and 20 $M_\odot$ stars of the same composition and $\alpha_1 = 0.015$, together with the data for the WNL and WNE stars observed by Hamann et al. (1993). There is an immediate new result coming out of this comparison, i.e. a new avenue for the formation of faint single WR stars ($\log L/L_\odot \sim 4 - 4.5$). Contrary to what suggested in the past, most likely the progenitors of the low luminosity WR stars are not the massive stars (say $M > 60$ $M_\odot$) evolving "*vertically*" in the HRD, but the less massive stars (say 15-20 $M_\odot$) evolving "*horizontally*" provided they suffered from significant mass-loss during the RSG phase (see Vanbeveren 1995). Soon after the RGB stages, the models are structurally similar to WNL stars, but they become visible as such only near the main sequence, when the effective temperature is high enough to show the spectral signatures of WR stars. Are the tiny envelopes of these WR candidates unstable and prone to the high mass-loss typical of WR stars? Answering this question deserves further investigation.

Acknowledgements. The authors thanks financial support from the Italian Ministry of University, Scientific Research and Technology (MURST), the Italian Space Agency (ASI), and the European Community under TMR grant ERBFMRX-CT96-0086. C.C. is pleased to acknowledge the hospitality and stimulating environment provided by ESO in Garching where this paper was written up during sabbatical leave from the Astronomy Department of the Padua University.

References

Abbott D.C., 1982, ApJ 259, 282
Alongi M., Bertelli G.P., Bressan A.G., Chiosi C., 1991, A&A 244, 95
Alongi M., Bertelli G.P., Bressan A.G., et al., 1993, A&AS 97, 851
Bertelli G.P., Bressan A.G., Chiosi C., 1984, A&A 130, 279
Bowen G.H., Willson L.A., 1991, ApJ 375, L53
Bressan A.G., 1994, Space Sci. Rev. 66, 373
Bressan A.G., Bertelli G.P., Chiosi C., 1981, A&A 102, 25
Bressan A.G., Fagotto F., Bertelli G., Chiosi C., 1993, A&AS 100, 647
Bressan A.G., Granato G.L., Silva L., 1998, A&A 332, 135
Caloi V., Cassatella A., Castellani V., Walker A., 1993, A&A 271, 109
Canuto V.M., 1992, ApJ 392, 218
Canuto V.M., 1994, ApJ 428, 729
Canuto V.M., 1996, ApJ 467, 385
Canuto V.M., Mazzitelli I., 1991, ApJ 370, 295
Castor J.I., Abbott D.C., Klein R.I., 1975, ApJ 195, 157
Charbonnel C., Meynet G., Maeder A., Schaller G., Schaerer D., 1993, A&AS 101, 415
Chiosi C., 1997, In: Aparicio A.J., Herrero A. (eds.) Stellar Astrophysics for the Local Group: a First Step to the Universe. Cambridge University Press
Chiosi C., Maeder G.A., 1986, ARA&A 24, 329
Chiosi C., Summa C., 1970, Astro. Space Sci. 8, 478
Chiosi C., Nasi E., Sreenivasan S.R., 1978, A&A 63, 103
Chiosi C., Bertelli G., Bressan A.G., 1992, ARA&A 30, 235
Chiosi C., Wood P.R., Capitanio N., 1993, ApJS 86, 541
Chiosi C., Vallenari A., Bressan A., Deng L., Ortolani S., 1995, A&A 293, 710
de Jager C., Nieuwenhuijzen H., van der Hucht K.A., 1988, A&AS 72, 295
de Koter A., Heap S., Hubeny I., 1997, ApJ 477, 792
Deng L., 1993, Ph.D. Thesis, ISAS, Italy
Deng L., Bressan A., Chiosi C., 1996a, A&A 313, 145
Deng L., Bressan A., Chiosi C., 1996b, A&A 313, 159
Eryurt D., Kirbiyik H., Kiziloglu N., Civelek R., Weiss A., 1994, A&A 282, 485
Fagotto F., Bressan A., Bertelli G., Chiosi C., 1994, A&AS 105, 39
Feast M.W., 1991, In: de Jager C., Nieuwenhuijzen H. (eds.) Instabilities in Evolved Super and Hyper-Giants.
Fitzpatrick E.L., Bohannan B., 1993, ApJ 404, 734
Freytag B., Ludwig H.H., Steffen M., 1996, A&A 313, 497

Gabriel M., 1995, In: Noels A., et al. (eds.) Stellar Evolution: What Should Be Done. 32th Liege International Astrophysical Colloquium, Inst. d'Astrophysique, Liege
Gail H.P., Sedlmayr E., 1987, A&A 171, 197
Grossman S., 1996, MNRAS 279, 305
Grossman S., Narayan R., 1993, ApJS 89, 361
Grossman S.A., Taam R.E., 1996, MNRAS 283, 1165
Grossman S., Narayan R., Arnett D., 1993, ApJ 407, 284
Habing H.J., Tignon J., Tielens A.G.G.M., 1994, A&A 286, 523
Hamann W.R., Koesterke L., Wessolowski U., 1993, A&A 274, 397
Heger A., Jeannin L., Langer N., Baraffe I., 1998, A&A 327, 224
Herrero A., Kudritzki R.P., Vilchez J., et al., 1992, A&A 261, 209
Herwig F., Blocker T., Schonberner D., Eid M.E., 1997, A&A 324, 81
Hillier D.J., 1996, In: Jeffery U.H.S. (ed.) Hydrogen Deficient Stars. 2nd International Colloquium, ASP Conf. Ser.
Ivezic Z., Elitzur M., 1995, ApJ 445, 415
Jura M., 1986, ApJ 303, 327
Jura M., Kleinmann S.G., 1990, ApJS 73, 769
Kato S., 1966, PASJ 18, 374
Kudritzki R.P., 1997, In: Aparicio A.J., Herrero A. (eds.) Stellar Astrophysics for the Local Group: a First Step to the Universe. Cambridge University Press
Kudritzki R.P., Gabler R., Groth H.G., Pauldrach A.W., Puls J., 1989, In: IAU Colloquium 113, p. 67
Kwok S., 1975, ApJ 1908, 583
Lafon J-P.J., Berruyer N., 1991, A&AR 2, 249
Lamers H., Cassinelli J., 1996, ASP Conf. Ser. 98, 162
Langer N., 1989, A&A 210, 93
Langer N., 1991, A&A 252, 669
Langer N., Sugimoto D., Fricke K.J., 1983, A&A 126, 207
Langer N., Eid M.F.E., Fricke K.J., 1985, A&A 145, 179
Langer N., Eid M.F.E., Baraffe I., 1989, A&A 224, 17
Lauterborn D., Refsdal S., Weigert A., 1971, A&A 10, 97
Lennon D.J., Dufton P.L., Mazzali P.A., Pasian F., Marconi G., 1996, A&A 314, 243
Lucy L.B., Solomon P.M., 1970, ApJ 159, 879
Maeder A., 1990, A&AS 84, 139
Maeder A., Conti P.S., 1994, ARA&A 32, 227
Maeder A., Meynet G., 1994, A&A 287, 803
Massey P., 1997, In: Aparicio A.J., Herrero A. (eds.) Stellar Astrophysics for the Local Group: a First Step to the Universe. Cambridge University Press
Massey P., Armandroff T., Pyke R., 1995a, AJ 110, 2715
Massey P., Lang C.C., DeGioia-Eastwood K., Germany C., 1995b, ApJ 438, 188
Merryfield W., 1995, ApJ 444, 318
Meynet G., Maeder A., Schaller G., Schaerer D., Charbonnel C., 1994, A&AS 103, 97
Pijpers F.P., Habing H.J., 1989, A&A 215, 334
Pijpers F.P., Hearn A.G., 1989, A&A 209, 198
Owocki S.P., Castro J.I., Rybicki G.B., 1988, ApJ 335, 914
Pauldrach A., Puls J., Kudritzki R.P., 1986, A&A 164, 86
Reid N., Tinney C., Mould J., 1990, ApJ 348, 98
Schaerer D., 1996, A&A 309, 129
Schaerer D., Charbonnel C., Meynet G., Maeder A., Schaller G., 1993, A&AS 102, 339
Schwarzschild M., Harm R., 1965, ApJ 142, 855
Talon S., Zahn J.P., Maeder A., Meynet G., 1997, A&A 322, 209
Vallenari A., Ortolani S., Chiosi C., 1994, A&AS 571, 108
Vanbeveren D., 1995, A&A 294, 107
Vassiliadis E., Wood P.R., 1993, ApJ 413, 641
Venn K.A., 1995, ApJ 449, 838
Ventura P., Zappieri A., Mazzitelli I., D'Antona F., 1998, A&A 334, 953
Weaver T.A., Woosley G.B., 1978, ApJ 225, 1021
Willson L.A., 1988, In: Stallion R., Willson L.A. (eds.) Pulsation and mass loss in Stars. Reidel, Dordrecht, p. 285
Willson L.A., Bowen G.H., Struck C., 1995, BAAS 187, 103
Xiong D.R., 1979, Acta Astron. Sin. 20, 238
Xiong D.R., 1984, Sci. Sinica 24, 1406
Xiong D.R., 1985, A&A 150, 133
Xiong D.R., 1989, A&A 213, 176
Zahn J.P., 1991, A&A 252, 179